Continuum Mech. Thermodyn. (2019) 31:101–132
https://doi.org/10.1007/s00161-018-0668-0

ORIGINAL ARTICLE

Patrick Franciosi · Mario Spagnuolo · Oguz Umut Salman

Mean Green operators of deformable fiber networks embedded in a compliant matrix and property estimates

Received: 14 October 2017 / Accepted: 13 April 2018 / Published online: 24 April 2018

Abstract Composites comprising included phases in a continuous matrix constitute a huge class of metamaterials, whose effective properties, whether they be mechanical, physical or coupled, can be selectively optimized by using appropriate phase arrangements and architectures. An important subclass is represented by "network-reinforced matrices," say those materials in which one or more of the embedded phases are co-continuous with the matrix in one or more directions. In this article, we present a method to study effective properties of simple such structures from which more complex ones can be accessible. Effective properties are shown, in the framework of linear elasticity, estimable by using the global mean Green operator for the entire embedded fiber network which is by definition through sample spanning. This network operator is obtained from one of infinite planar alignments of infinite fibers, which the network can be seen as an interpenetrated set of, with the fiber interactions being fully accounted for in the alignments. The mean operator of such alignments is given in exact closed form for isotropic elastic-like or dielectric-like matrices. We first exemplify how these operators relevantly provide, from classic homogenization frameworks, effective properties in the case of 1D fiber bundles embedded in an isotropic elastic-like medium. It is also shown that using infinite patterns with fully interacting elements over their whole influence range at any element concentration suppresses the dilute approximation limit of these frameworks. We finally present a construction method for a global operator of fiber networks described as interpenetrated such bundles.

Keywords Composites · Fiber networks · Green operator · Effective properties · Phase co-continuity

1 Introduction

Particular attention is paid in this work to those composite structures in which the domains that are embedded in a homogeneous matrix can be considered as infinite fibers of a same second phase, as exemplified in Fig. 1. They are assumed to be arranged such as to make either a one-directional bundle or interpenetrated ones along several directions of space, so realizing various sorts of lattice network in 1, 2 or 3 dimensions, the modeling of which, in terms of effective property estimate, is still highly challenging, owing to the phase

Communicated by Francesco dell'Isola.

P. Franciosi (✉) · M. Spagnuolo · O. U. Salman
LSPM UPR 3407 CNRS, University of Paris13, USPC, 93430 Villetaneuse, France
E-mail: patrick.franciosi@univ-paris13.fr

M. Spagnuolo
E-mail: mario.spagnuolo@lspm.cnrs.fr

O. U. Salman
E-mail: umut.salman@lspm.cnrs.fr

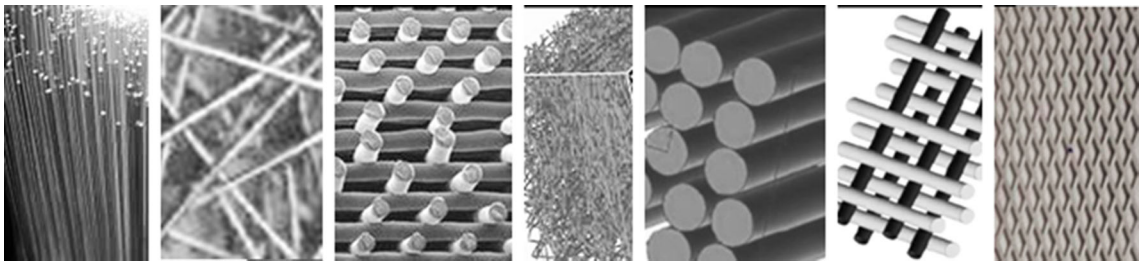

Fig. 1 Some (dimensionless) examples of 1-directional (1D) fiber bundles and of 2D and 3D fiber networks

co-continuity [1–6]. Whether it be random or periodically ordered, a one-directional bundle of infinite fibers makes the composite medium bi-continuous in the fiber direction and phase co-continuity is ensured in all fiber directions of multi-directional such networks which are through-sample spanning. Such networked fiber structures can be found in many different materials the matrix phase of which can have different (elasto-visco-plastic) behavior types, including possible damage, and in most cases the fiber phase combines both stretching and bending straining modes at least in some ranges of deformation [7–11], while the network itself is more or less deformable according to the nature of the interconnections between its elements. These structures also include as particular class the so-called pantographic structures (Fig. 1 right), which have common features with the other networks here of concern, as far as they behave as a classic first gradient material [12] and although they may become governed by extremely nonlinear equations under various deformation ranges and modes [13–19]. It is noteworthy that these particular objects and similar ones, firstly introduced in [20], are nowadays of primary importance both in applications and for fundamental purposes regarding the study of generalized continua and, in the specific, of second gradient materials [21]. Here, this first step in the investigation of effective property estimates for matrices reinforced with fiber networks will be restricted to purely elastic regime, and bending mode analyses are delayed to subsequent works. Extensions to accounting for the emerging of effects due to plasticity are also possible, in different ways, as, for example, following the early works presented in [22–26], an analysis applied by the authors to simple systems of beams. This can likely be generalized to the composites here of concern and possibly extended up to damage onset, but all this is out of the present scope.

Now, when in heterogeneous structures of the general (inclusion or fiber) reinforced matrix type (which can be found at many different scales from micro-mechanics to macro-engineering problems as for examples embedded tanks or dug tunnels in soils subjected to seismic loading[1]) the embedded domains are too dense in the matrix, the interactions between these domains cannot be disregarded in the estimation of some effective properties. The network-reinforced matrices here of concern suffer the specific difficulty that in addition to classical pair interaction effects between elements, changes in the network structure can be important, what is likely to further affect the interactions in return. For example, thanks to a compliant matrix and also depending on various possible interconnections between elements (from simple contacts to physical links), the network elements are likely to significantly change their orientations and their inter-distances under straining, so deserving to currently account for the interaction changes.

How much pair interactions in clusters of inclusions or fibers affect the overall material behavior remains an open question. The fact that only the nearest neighbors to an inclusion are in practice considered to significantly matter has been pointed as excessively simplifying, even when no long-range order exists [30]. For embedded domains that become aligned and get close to each other when, for example, the embedding matrix is soft enough to suffer a large deformation, interactions may become of non-negligible effect even if the embedded domains are initially in quite dilute concentration. In some circumstances, when, for example, the interactions between domains increase in certain directions and oppositely decrease and vanish in other ones, it is certainly important to account for the current evolution of the interactions in estimating effective properties of composites and meta-materials. These interactions are not that easy to estimate. They can be accounted for either in some average or statistical way (as is the case in self-consistent schemes [31–33] or in statistical approaches [34,35] for random structures) or in fully deterministic manner, from the calculation of the interaction Eshelby tensors or related operators [36,37] between all element pairs in a pattern, when there is some particular organization of the elements.

[1] See, such applicative examples at geo-mechanical level in the references [27–29].

In many homogenization frameworks, the main role to estimate effective properties of heterogeneous structures is carried by the Eshelby tensors [38], say $\mathbf{E}^V(\mathbf{r})$, that relate, in a medium, the constrained strains $\boldsymbol{\varepsilon}^{*V}(\mathbf{r})$ at points interior or in the vicinity of some finite domain V to an assigned stress-free-strain (eigenstrain) $\boldsymbol{\varepsilon}^0$ in it, as $\boldsymbol{\varepsilon}^*(\mathbf{r}) = \mathbf{E}^V(\mathbf{r}):\boldsymbol{\varepsilon}^0$. (These domains V represent either elements of embedded phases or a particular distribution or organization symmetry of these phases in the medium.) In cases when a domain V does not represent a single inclusion but a pattern of them, the Eshelby tensor at any point of each element Vi of V comprises the interior contribution of that element and all the exterior ones from the other elements of V. Similarly, the average Eshelby tensor interior to a pattern of N elements $V = \bigcup_{i=1}^{N} Vi$, say $\overline{\mathbf{E}^V}$(such that $\overline{\boldsymbol{\varepsilon}^{*V}} = \overline{\mathbf{E}^V}:\boldsymbol{\varepsilon}^0$ is the mean constrained strain in the pattern V due to $\boldsymbol{\varepsilon}^0$ assigned in it), comprises, in appropriately weighed sum, the mean interior tensors of the elements Vi and the mean interaction tensors between all element pairs constituting the pattern. While the interior Eshelby tensor is already not easily at hand for any general V domain shape even in the simplest cases of a matrix with isotropic properties, the interaction tensor between domain pairs is even harder to access, which makes difficult to obtain the global tensor of a specific pattern. Yet, in order to estimate effective properties of reinforced matrices, it is frequently enough to explicate, rather than the entire Eshelby tensor field over V, the mean tensor form which is generally of easier access. Now, the so-called modified Green operator integral, say $\mathbf{t}^V(\mathbf{r})$, is the product $\mathbf{E}^V(\mathbf{r}):\mathbf{C}^{-1}$ between the Eshelby tensor and the compliance (inverse stiffness) tensor $\mathbf{C}^{-1}$ of the medium (the matrix) in which V is embedded. This operator relates the constrained strains $\boldsymbol{\varepsilon}^{*V}(\mathbf{r})$ at points interior or in the vicinity of V to the assigned eigenstress (or polarization stress) $\boldsymbol{\tau}^0 = \mathbf{C}:\boldsymbol{\varepsilon}^0$ in it. Again, if a mean global operator of V can be considered, then it simply follows that $\overline{\mathbf{E}^V}:\mathbf{C}^{-1} = \overline{\mathbf{t}^V}$. The knowledge of $\mathbf{t}^V(\mathbf{r})$ is then quite equivalent to the knowledge of $\mathbf{E}^V(\mathbf{r})$ but using $\mathbf{t}^V(\mathbf{r})$ (and $\overline{\mathbf{t}^V}$) operators instead of $\mathbf{E}^V(\mathbf{r})$ (and $\overline{\mathbf{E}^V}$) tensors has advantages that have been already presented in previous works on similar problems [6–35,39,40]. Major ones are the positive-definiteness and the super-symmetry properties of the modified Green operators that the Eshelby tensors do not have.

We here use for short the terms “interior”, “pair interaction” and “global interaction” operator, to name, respectively, the mean (or uniform when so) modified Green operator integral representative of an embedded domain in a matrix, the mean interaction operator integral between any two such embedded domains and the whole mean interaction operator integral within a pattern of several domains.

A large variety of morphological situations involving complex patterns can nowadays be approached (in terms of both interior and interaction operators) by using numerical tools. However, analytical solutions, if simply accessible, remain the preferential way to approach these “inclusion problems”, owing to the easier manipulation of closed-form solutions when any. Following this central idea, the analytical solution for the key pair interaction problem, in terms of Green operators, between two general ellipsoids has been treated formally in [39–42]. In [42] the geometrical features of the Radon transform (RT) and inverse transform (IRT) method [43–46], which were previously used only in part, as in [47–49], are developed for obtaining simple operator forms for various inclusion or pattern shapes. In the literature also the symmetry properties of the matrix have been well investigated [50–54] in order to approach more general varieties of problems. In the last years, the RT/IRT method has been applied to several non-ellipsoidal domains and domain patterns, providing quite simple analytical forms for the mean global operator of the domains, for the mean pair interaction operators between each two elements in them and/or for the global interaction part of patterns [36,37,55–57].

In this context, the specific interests of knowing and using mean operators of large, infinite-like, patterns, as those obtained in earlier already cited works for spheres, spheroids or finite cylinder alignments will be shown herein, using the example of bundles of infinite parallel cylinders. It will be shown that only a finite part of infinite patterns contributes to the global interaction, owing to an influence distance (that we determine) beyond which interactions between elements become negligible. On the contrary to a domain that represents a spatial distribution of inclusions or of patterns within which the element arrangement will somehow also evolve with their spatial distribution, this influence (or interaction cutoff) distance defines (unless changes in the matrix symmetry properties) a size- and shape-invariant influence zone around any element and circumscribes a finite yet varying part of the infinite pattern.

The present work aims at being a preliminary examination of interpenetrated fiber bundles with the goal of arriving, in a forthcoming paper, at describing more complex embedded networks in compliant matrices for effective property estimates from classical mean field homogenization framework (say, no second gradient theory) to begin with. It will be pointed that the concept of infinite patterns suffering element interactions over a finite and invariant influence zone has specific interest for continuous fiber networks in which by definition a

finite pattern cannot be specified while an interaction domain of finite size can be introduced. Damage features as matrix fracture or interface debonding will be disregarded.

The access to interaction estimates between the elements of such fiber networks in the homogenization context imposes to at first solve analytically the interaction problem between two infinite parallel fibers with same cross section. Surprisingly, the basic case of parallel infinite fibers with circular cross sections is not present in explicit form in the literature so far, to the authors knowledge, even for cylinders of same cross section radius, and although the single cylindrical inclusion case has been already treated [58,59]. It is noteworthy (as shown next on) that from the RT/IRT method, this one-cylinder problem is solved (say the cylinder Green operator is obtained) in a simple manner and no calculations.

In this article, we thus start by fully solving this two-cylinder basic problem (say providing the mean global cylinder pair Green operator), a quite tedious mathematical exercise reported will all required details in an "Appendix" that fortunately ends with a quite simple operator form. From this firstly solved case, the exact analytical solution for the mean global Green operator of n-planar alignments of parallel infinite cylinders (up to infinite fiber number) is presented, in a quite simple derivation from the pair interaction operator.[2] It is then shown how to obtain from these operators for planar alignments the operator solution for infinite one-directional bundles of parallel infinite cylinders and how the latter allows, in terms of effective properties, applications for embedded structures of interpenetrated bundles.

Now, in order to show how, with these available mean operators for infinite patterns, one can describe quite simply effective properties for the sorts of deformable fiber networks we are concerned with and how one can follow the effective property evolutions resulting from deformation of the fiber arrangement, a homogenization framework is necessary. Among the most simple (mean field, first gradient) homogenization frameworks which are likely to be used for such property estimates (see [60–63] for reviews), we will make use of the framework of Ponte-Castaneda and Willis (PC-W) [34], a type of mean field approximation which has also been shown to apply for patterns in [35,37,57,61,64]. While the validity of these homogenization frameworks is generally considered restricted to dilute inhomogeneity concentrations since the interactions are not, or not sufficiently, accounted for, the application to finite patterns allows the account of the interactions interior to the pattern (even when made of several phases, as in [65]). But estimates employing finite patterns still are restricted to dilute concentrations of the selected pattern, with the interactions between the patterns remaining to be improved for large concentrations. If when the larger is the representative pattern the lower is the disregarded interaction part, the use of infinite-like patterns with all interior pair interactions possibly accounted for at any concentration of the elements is expected to substantially correct, if not suppress, these dilute approximation restrictions. It will be shown that the PC-W estimate form remains relevant at the limit of infinite representative patterns when the representative spatial distribution symmetry is taken to be the one of the influence (interaction) domains.

Additionally, in order to describe structures with multi-directionally continuous fiber networks (inter penetrated bundles) in a continuous matrix, for which the PC-W framework is not appropriate, we will also refer to the so-called fiber systems introduced in [1–4] as well as to the laminate systems inspired from them, as presented in [5,6].

Section 2 recalls briefly the RT/IRT method and the generic solution for the interaction operator between two ellipsoids both already presented in several earlier works. Main details of the RT/IRT method are nevertheless recalled in "Appendix A". The (original) analytical calculations of the mean interaction operator between two infinite parallel cylindrical fibers, which are reported in "Appendix B" with the necessary details for allowing calculation checking and applications, result from specializing the ellipsoid pair to treat the limit case of two infinitely long identical spheroids. Section 3 presents the analytical solution for the global operator of a planar alignment of n infinite parallel cylinders, with n from 2 to infinity that results from the knowledge of the pair interaction operator. Section 4 presents typical deformable fiber bundles and networks we are interested in and compares some property estimates from using the global operators for the infinite networks obtained from the alignment operators with estimates using operators of finite patterns. The key role and helpfulness of the mean operator of infinite planar alignments of parallel fibers to follow the main arrangement changes in these fiber patterns are shown from comparing with a few numerical simulations that are also provided in support. The extension principle to 2D and 3D fiber networks described as interpenetrated directional 1D bundles is also exemplified in Sects. 4, and 5 briefly concludes.

[2] The also obtained solution for similar mean operators of planar alignments of beams with any rectangular cross section is to appear in [57].

2 The mean characteristic functions and Green operators of an inclusion pair from the IRT

2.1 Brief summary of the general IRT framework

We consider an infinite medium (matrix) with property tensor[3] $\mathbf{C}$ containing a V inclusion, which is any general, piecewise regular, possibly multiply connected, bounded domain. As recalled in "Appendix A" from earlier works [36,42] and other following ones that are also cited herein, the modified Green operator $\boldsymbol{\Gamma}(\mathbf{r}-\mathbf{r}')$ we are concerned with results from the double x-differentiation at point $\mathbf{r} = (x_1,\ x_2,\ x_3)$ in the medium (when explicating the stress equilibrium conditions) of the $\mathbf{G}(\mathbf{r}-\mathbf{r}')$ Green function that relates an applied punctual force field at a point $\mathbf{r}'$ to the displacement field it creates at $\mathbf{r}$. The integral over that domain V of $\boldsymbol{\Gamma}(\mathbf{r}-\mathbf{r}') = -\partial^2\mathbf{G}(\mathbf{r}-\mathbf{r}')/\partial x_p \partial x_q$ yields the operator $\mathbf{t}^V(\mathbf{r}) = \int_V \boldsymbol{\Gamma}(\mathbf{r}-\mathbf{r}')\ \mathrm{d}\mathbf{r}'$ at interior points $\mathbf{r}$ of V and its mean interior value over V, $\overline{\mathbf{t}^V} = \frac{1}{v}\int_V \mathbf{t}^V(\mathbf{r})\mathrm{d}\mathbf{r}$. From the RT/IRT method in R^3, the form of the interior operator $\mathbf{t}^V(\mathbf{r})$ (resp. of the mean operator $\overline{\mathbf{t}^V}$ over V) is a weighted angular average of elementary operators $\mathbf{t}^P(\boldsymbol{\omega})$ over the vectors $\boldsymbol{\omega} = (\theta, \phi)$ of the unit sphere Ω (θ being counted around the x_3 axis and ϕ from axis x_1 in the (x_1, x_2) plane in all what follows). After recalled manipulations in "Appendix A", this results in writing for the elastic-like cases,[4] with $\boldsymbol{\omega} = (\sin\theta\cos\phi, \sin\theta\sin\phi, \cos\theta)$, $d\boldsymbol{\omega} = \sin\theta d\theta d\phi$:

$$t^V_{pqjn}(\mathbf{r}) = \int_V \Gamma_{pqjn}(\mathbf{r}-\mathbf{r}')\ \mathrm{d}\mathbf{r}' = \int_\Omega \psi_V(\omega, \mathbf{r})\ t^P_{pqjn}(\omega)\ d\omega \tag{1}$$

where:

$$t^P_{pqjn}(\boldsymbol{\omega}) = \left((M^{-1})_{pj}(\boldsymbol{\omega})\omega_q\ \omega_n\right)_{(pq),(jn)} \quad ; \quad M_{mp}(\boldsymbol{\omega}) = C_{mipj}\omega_j\ \omega_i, \tag{2}$$

$$\psi_V(\boldsymbol{\omega}, \mathbf{r}) = \frac{1}{8\pi^3}\int_V (-\pi)\,\delta''\left(\boldsymbol{\omega}.\left(\mathbf{r}-\mathbf{r}'\right)\right)\mathrm{d}\mathbf{r}' = -\frac{s_{V''}(z,\omega)}{8\pi^2}. \tag{3}$$

The rank-four elementary Green operators in Eq. (2) are super-symmetric and so it is as well for the Green operator of any V domain, what is not the case for the related Eshelby tensors.[5] From the IRT, the mean interior operator for V takes the form $\overline{\mathbf{t}^V} = \int_\Omega \overline{\psi_V}(\boldsymbol{\omega})\ \mathbf{t}^P(\boldsymbol{\omega})\mathrm{d}\boldsymbol{\omega}$. For $\mathbf{t}^V(\mathbf{r})$ (resp. $\overline{\mathbf{t}^V}$), $\psi_V(\boldsymbol{\omega}, \mathbf{r})$ (resp. $\overline{\psi_V}(\boldsymbol{\omega}) = \frac{1}{v}\int_V \psi_V(\boldsymbol{\omega}, \mathbf{r})\mathrm{d}\mathbf{r}$) is the weighting function for the elementary operators $\mathbf{t}^P(\boldsymbol{\omega})$ which, in the case of a matrix with isotropic properties, reduce to simple trigonometric functions as recalled in "Appendix B". In Eq. (3), $s_V(z, \boldsymbol{\omega})$ is the section area of V by the plane of equation $z = \boldsymbol{\omega}.\mathbf{r}$, of $\boldsymbol{\omega}$-normal, which passes through $\mathbf{r}$ and $s_{V'}(z, \boldsymbol{\omega})$, $s_{V''}(z, \boldsymbol{\omega})$ are the first and second z-derivatives of $s_V(z, \boldsymbol{\omega})$, say $\frac{\partial^{(i)}s_V(z,\boldsymbol{\omega})}{\partial z(\boldsymbol{\omega})^i}$, $i = 1, 2$. For a "smooth enough" boundary ∂V of the domain V,[6] one can equivalently write $\forall\boldsymbol{\omega}$:

$$\overline{\psi_V}(\boldsymbol{\omega}) = \frac{1}{v}\int_{d_V^-}^{d_V^+}\left(s_{V''}(z) - \sum_{i=1,2}\left(s_{V'}(d_i^V)\delta(\pm z - d_i^V)\right)\right)s_V(z)\mathrm{d}z = -\frac{1}{v}\int_{d_V^-}^{d_V^+}(s_{V'}(z))^2\mathrm{d}z. \tag{4}$$

By definition for the interior weight function of V, its integral over the unit sphere is normalized as $\int_\Omega \psi_V(\omega, \mathbf{r})\ \mathrm{d}\omega = \int_\Omega \overline{\psi_V}(\boldsymbol{\omega})\mathrm{d}\boldsymbol{\omega} = 1$. If V is an infinite fiber, the breadth is infinite and the weight function is zero in all directions except normally to the fiber axis. For a x_3-cylinder, the breadth around the x_3 axis is isotropic and the weight function value around x_3 fulfills $\int_\theta\int_\phi \psi_{\mathrm{cyl}}(\theta, \phi)\ \sin\theta\mathrm{d}\theta\mathrm{d}\phi\ = \psi_{\mathrm{cyl}}\int_{\phi=0,2\pi}\ \mathrm{d}\phi = 1$, say $\psi_{\mathrm{cyl}}(0, \phi) = 1/2\pi, \forall\phi$.

When in the right hand side of Eq. (4), V is an inclusion pair such that $V = V1 \cup V2$ ($V1 \cap V2 = \emptyset$), one has $s_{V'}(z, \boldsymbol{\omega}) = s_{V1'}(z, \boldsymbol{\omega}) + s_{V2'}(z, \boldsymbol{\omega})$, and the mean weight function of V shares into two mean (or uniform for ellipsoids) interior weight functions $\overline{\psi_{V1}}(\boldsymbol{\omega})$ and $\overline{\psi_{V2}}(\boldsymbol{\omega})$, corresponding to the terms $\left(s_{V1'}(z)\right)^2$ and $\left(s_{V2'}(z)\right)^2$ for the elements $V1$ and $V2$ plus the two mean cross-interaction parts $\overline{\psi_V^{V1-V2}}(\boldsymbol{\omega})$ and $\overline{\psi_V^{V2-V1}}(\boldsymbol{\omega})$

[3] Although elastic properties are of first concern here, all holds as well for four-rank elastic-like (including the so-called generalized elasticity type in the case of coupled magneto-electro-elastic properties) properties or second-rank dielectric-like ones [66].

[4] Which contain the dielectric-like cases as subcase [36,56].

[5] The super-symmetric Green operators have left, right and super-skew-symmetric counterparts, the left one of which matters for example when domain rotations need to be accounted for [32].

[6] If V is a pattern ($V = \cup Vi$), ∂V here stands for $\cup\partial Vi$ and the breadth of a pattern is the breadth of its convex hull.

both corresponding to the cross-product $s_{V1'}(z,\boldsymbol{\omega})s_{V2'}(z,\boldsymbol{\omega})$. When the two inclusions are congruent to some $V0$ shape, as is the case in the here treated inclusion pairs, the sum of the two mean (or uniform for ellipsoids) interior weight functions is exactly the (mean or uniform) interior weight function $\overline{\psi_{V0}}(\boldsymbol{\omega})$ of the shape $V0$. We call "interaction part" in the weight function the ensemble of the two cross- interaction parts, say $\overline{\psi_V^{V1,V2}}(\boldsymbol{\omega}) = \overline{\psi_V}(\boldsymbol{\omega}) - \overline{\psi_{V0}}(\boldsymbol{\omega})$. Since by definition both $\int_\Omega \overline{\psi_V}(\boldsymbol{\omega})\mathrm{d}\boldsymbol{\omega} = 1$ and $\int_\Omega \overline{\psi_{V0}}(\boldsymbol{\omega})\mathrm{d}\boldsymbol{\omega} = 1$, it comes $\int_\Omega \overline{\psi_V^{V1,V2}}(\boldsymbol{\omega})\mathrm{d}\boldsymbol{\omega} = 0$. All these generalities for inclusion pairs extend to n-inclusion patterns. The overall mean interaction operator in a pattern is the total of the appropriately weighted mean pair interaction terms.

2.2 Application to pairs of identical congruent spheroids

The mean pair interaction operator $\overline{\mathbf{t}_V^{V1,V2}} = \int_\Omega \overline{\psi_V^{V1,V2}}(\boldsymbol{\omega})\mathbf{t}^P(\boldsymbol{\omega})\mathrm{d}\boldsymbol{\omega}$ between two general inclusions, $V1$ and $V2$, as introduced in [42] for ellipsoids, is the cross-part of the global interior mean operator $\overline{\mathbf{t}^V}$ for the domain $V = V1 \cup V2$ ($V1 \cap V2 = \emptyset$), of volume $v = v1 + v2$ and reads:

$$\overline{\mathbf{t}^V} = \frac{1}{v}\sum_{i=1,2}\sum_{j=1,2}\int_{Vi}\int_{Vj}\boldsymbol{\Gamma}(\mathbf{r}-\mathbf{r}')\mathrm{d}\mathbf{r}'\mathrm{d}\mathbf{r} = \frac{v1}{v}\overline{\mathbf{t}^{V1}} + \frac{v2}{v}\overline{\mathbf{t}^{V2}} + \overline{\mathbf{t}_V^{V1,V2}}. \tag{5}$$

For $V1$ and $V2$ congruent to a same $V0$ shape one has for the interior operator parts, similarly to the weight function parts $\frac{v1}{v}\overline{\mathbf{t}^{V1}} + \frac{v2}{v}\overline{\mathbf{t}^{V2}} = \overline{\mathbf{t}^{V0}}$. We now on specialize to pairs of spheroids.

In contrast to previously considered axially symmetric inclusion pairs and patterns with regard to the x_3 axis ($\theta = 0$), we here consider two congruent spheroids $V1$, $V2$, of x_2-oriented symmetry axis (Fig. 2), say ($\theta = \pi/2$, $\varphi = \pi/2$) and lying in plane $x_2{-}x_3$. The calculations, according to the RT/IRT method, for the mean pair interaction weight function and operator between two parallel identical spheroids of radius cross section R at the limit of 2 infinite cylinders with axis inter-distance $2L$, are reported in "Appendix B" with the minimal information for allowing mathematical check and easy use.

All calculations done, one thus obtains for $\zeta \to \infty$ the needed independent two functions:

$$I^{1,0}_{2\mathrm{cyl}\infty} = C_2 = \sum_{i(m,n)=1}^{3} \zeta^\infty I^{1,0}_{i(m,n)} = -\frac{\rho_0^2}{10};\ I^{2,0}_{2\mathrm{cyl}\infty} = C_4 = \sum_{i(m,n)=1}^{3} \zeta^\infty I^{2,0}_{i(m,n)} = -\frac{\rho_0^2}{20} - \frac{9\rho_0^4}{280}, \tag{6}$$

in which $\rho_0 = R/L$ and from which the three other involved trigonometric functions result as $S_2 = -I^{1,0}_{2\mathrm{cyl}\infty}$, $S_2C_2 = I^{1,0}_{2\mathrm{cyl}\infty} - I^{2,0}_{2\mathrm{cyl}\infty}$, $S_4 = I^{2,0}_{2\mathrm{cyl}\infty} - 2I^{1,0}_{2\mathrm{cyl}\infty}$. These 5 functions from Eq. (6), that are the first original

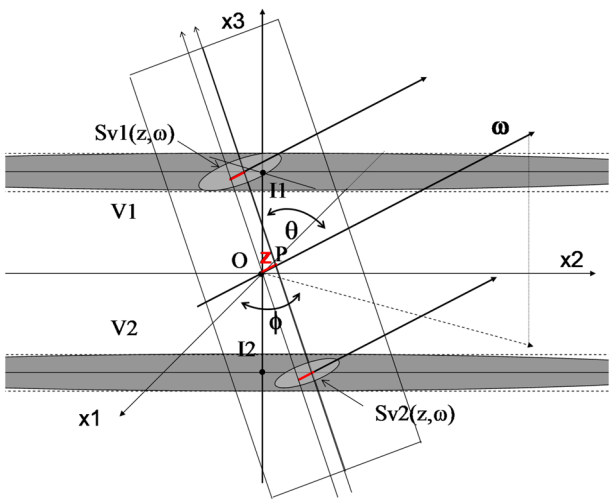

Fig. 2 Pair of $x2$-oriented parallel identical prolate (infinite-like) spheroids $V1$, $V2$ in plane $x_2{-}x_3$ and section areas by the plane of equation $z = \boldsymbol{\omega}.\mathbf{r}$

Table 1 Interior operator of η-elliptic $x2$-cylinder (col.1) and sphere (col.4); mean pair interaction operator for 2 circular $x2$-cylinder (col. 2 and 3) and spheres (col. 5) aligned along $x3$

	$x_2\eta$-elliptic cylinder interior $\mathbf{t}^{x_2\eta-\mathrm{cyl}}$	x_2 cylinder general pair interaction form	x_2 cylinder pair interaction form $\mathbf{v}0\rho_0^2+\mathbf{w}0\rho_0^4$	Sphere interior $\mathbf{t}^{\mathrm{sph}}$	Sphere pair interaction form $\mathbf{v}0\rho_0^3+\mathbf{w}0\rho_0^5$
1111	$\frac{(2+\eta)A}{2(1+\eta)^2}+\frac{B}{1+\eta}$	AS4 + BS2 = A(C4 − 2C2) − BC2	$\frac{2\|B\|-3\|A\|}{20}\rho_0^2+\frac{9\|A\|}{280}\rho_0^4$	$\frac{3A+5B}{15}$	$\frac{2\|B\|-3\|A\|}{48}\rho_0^3+\frac{3\|A\|}{160}\rho_0^5$
1122	0	0	0	$\frac{A}{15}$	$-\frac{\|A\|}{48}\rho_0^3+\frac{\|A\|}{160}\rho_0^5$
1133	$\frac{\eta A}{2(1+\eta)^2}$	AS2C2 = A(C2 − C4)	$\frac{\|A\|}{20}\rho_0^2-\frac{9\|A\|}{280}\rho_0^4$	$\frac{A}{15}$	$\frac{\|A\|}{24}\rho_0^3-\frac{4\|A\|}{160}\rho_0^5$
2222	0	0	0	$\frac{3A+5B}{15}$	$\frac{2\|B\|-3\|A\|}{48}\rho_0^3+\frac{3\|A\|}{160}\rho_0^5$
2233	0	0	0	$\frac{A}{15}$	$\frac{\|A\|}{24}\rho_0^3-\frac{4\|A\|}{160}\rho_0^5$
3333	$\frac{\eta(1+2\eta)A}{2(1+\eta)^2}+\frac{\eta B}{1+\eta}$	AC4 + BC2	$\frac{-2\|B\|+\|A\|}{20}\rho_0^2+\frac{9\|A\|}{280}\rho_0^4$	$\frac{3A+5B}{15}$	$-\frac{2\|B\|}{24}\rho_0^3+\frac{8\|A\|}{160}\rho_0^5$
2323	$\frac{\eta B}{4(1+\eta)}$	(B/4)C2	$-\frac{\|B\|}{40}\rho_0^2$	$\frac{2A+5B}{30}$	$\frac{4\|A\|-\|B\|}{96}\rho_0^3-\frac{4\|A\|}{160}\rho_0^5$
3131	$\frac{\eta A}{2(1+\eta)^2}+\frac{B}{4}$	AS2C2	$\frac{\|A\|}{20}\rho_0^2-\frac{9\|A\|}{280}\rho_0^4$	$\frac{2A+5B}{30}$	$\frac{4\|A\|-\|B\|}{96}\rho_0^3-\frac{4\|A\|}{160}\rho_0^5$
1212	$\frac{B}{4(1+\eta)}$	(B/4)S2 = − (B/4)C2	$\frac{\|B\|}{40}\rho_0^2$	$\frac{2A+5B}{30}$	$\frac{\|B\|-\|A\|}{48}\rho_0^3+\frac{\|A\|}{160}\rho_0^5$

theoretical result of this work, explicitly yield the terms of the mean pair interaction operator between two $x2$-oriented cylinders reported in Table 1, using the two constants $A=-0.5B/(1-v)$ and $B=1/\mu$ for isotropic elastic-like matrices of shear modulus μ and Poisson ratio v (or the single one $B=1/D$ for dielectric-like ones, with dielectric modulus D). The first column of Table 1 reports (from [56]) the interior operator for an x_2-oriented fiber of elliptic cross sections having their two axes along the x_1 and x_3 axes. The coefficient η is the "stretch" (ellipticity) in direction $x3$: infinite (resp. null) aspect ratio η yields the laminate operator with normal x_1 (resp. x_3). The interior operator of the single infinite x_2-oriented cylindrical fiber ($\eta=1$) is retrieved from using the first of the three elements of the integral in Eq. (A.3), taking $\theta\min(\varphi)=0$ (resp. $\mathrm{xmax}(\varphi)=1$), for all φ values, as the min (resp. max) integration bound, say $\rho_0=1$, what gives 1/2 and 3/8 for $p=1$ and $p=2$, respectively. Then, the terms of the global operator for the cylinder pair result from Table 1 for the x_2-oriented cylinders from adding the interior (at $\eta=1$) and the interaction operator and then for any orientation using the appropriate rotation matrix.

The sphere and sphere pair terms (from [36]) are also reported for comparison. Here, as the limit case when $\zeta=1$, they simply correspond to the θ or x integrals, with the φ-integrals simply multiplying the θ-integral results by a factor $(2/\pi)\int_0^{\pi/2}\cos^{2q}\phi\mathrm{d}\phi$, $q=0,1,2$).[7]

It is striking that although often tedious, the calculations for the fiber pair interaction finally yield a quite simple operator polynomial form in terms of the ratio $\rho_0=R/L$, with an obvious consistency with the previous results concerning alignments of spheres in [36], as is seen from Table 1. These analytical forms were not, to the authors knowledge, provided earlier in the literature. The dimensionless nonzero terms of the elasticity mean global (interior plus interaction) pair operator for parallel identical cylinders (say multiplied by the shear modulus μ) are plotted in Fig. 3 as a function of the normalized distance L/R and for Poisson ratio of 0.3 and 0.5 (incompressible limit case).

According to the introductive recalls, the $(ijkl)$ terms of a mean Green operator for an inclusion pattern V represent the mean of the constrained strain $(\varepsilon^*_{ij}(r))$ in V when it suffers a unit uniform polarization stress (τ^0_{kl}) according to the relation $\overline{\varepsilon^*_{ij}}=\overline{t^V_{ijkl}}\tau^0_{kl}$. And it is an essential operator for effective property estimates in composites as seen in Sect. 4. At large enough distance L, the interaction part vanishes and the global operator reduces to the interior one. It is seen from Fig. 3 that the influence or cutoff interaction distance is typically ten times the cylinder radius, with no significant effect of Poisson ratio in the range $v\in(0.3{-}0.5)$.

From Eq. (6), the terms of the pair interaction operator obey the even polynomial decomposition in ρ_0:

$$\overline{\mathbf{t}^{\mathrm{cyl,cyl}}_{\rho_0}}=\mathbf{v}0\rho_0^2+\mathbf{w}0\rho_0^4, \tag{7}$$

[7] The differences with the results in [36] come from an inter-distance definition difference where $\rho_0=2\rho$.

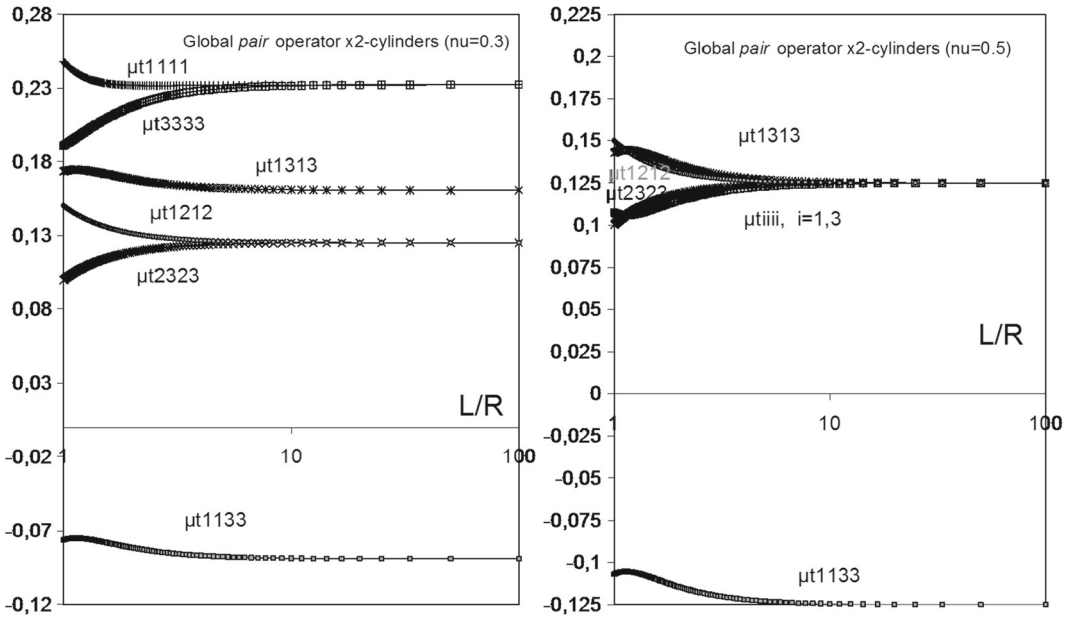

Fig. 3 Global (interior plus interaction) operator for two parallel infinite x_2-cylinders in plane of normal x_1

while for the sphere pair case it was of the odd form $\overline{\mathbf{t}^{\mathrm{sph,sph}}_{\rho_0}} = \mathbf{v}0\rho_0^3 + \mathbf{w}0\rho_0^5$ (with different tensors $\mathbf{v}0$, $\mathbf{w}0$). As for spheres, the $\mathbf{w}0$ part is only present for elastic-like material properties, in which case certain $(ijkl)$ components (when $v0_{ijkl}$ and $w0_{ijkl}$ have opposite signs) of the interaction operator can exhibit an optimum for $\rho_{0*} < 1$ which depends on the Poisson ratio through the A/B coefficient ratio.

The next section examines patterns of parallel infinite cylindrical fibers and gives their global mean operator in exact analytical form as well. This will show that while for a single pair of fibers the interaction part of a global pair operator can be considered as modest in view of the main interior contribution, the cumulated interaction contribution in large alignments becomes of the same order as the interior term when the fiber inter-distance is small.

3 General and planar patterns of identical parallel infinite cylindrical fibers

3.1 Mean operator of general patterns of n parallel cylinders

Take a fiber set $V = V1 \cup V2 \cup \cdots \cup Vn$, with $Vi \cap Vj = \emptyset, \forall i \neq j \in (1, n)$, regardless of the spatial arrangement of the fibers in the bundle. The operator at any $\mathbf{r}$ interior or exterior point of V (including exterior points which are interior to the convex hull of V) results from the superimposition of the elementary solutions for the involved n inclusions and the involved $C_2^n = \frac{n!}{2(n-2)!}$ pair interactions (for $n = 2$, there is one pair interaction, as defined to be the sum of the two opposite 1-2 and 2-1 terms). Similarly, the mean operator for V assembles all the mean pair interaction terms together with one interior operator under the form:

$$\overline{\mathbf{t}^{V}} = \sum_{i=1}^{n} \frac{vi}{v} \overline{\mathbf{t}^{Vi}} + \sum_{i=1}^{n} \sum_{j=i+1}^{n} \left(\frac{vi + vj}{v} \right) \overline{\mathbf{t}^{Vi,Vj}}, \text{ with } v = \sum_{i=1}^{n} vi. \tag{8}$$

All cylinders being infinite, one has $\sum_{i=1}^{n} \frac{vi}{v} \overline{\mathbf{t}^{Vi}} = \overline{\mathbf{t}^{V0}}$ (even if they are not all of same radius), with $\overline{\mathbf{t}^{V0}} = \mathbf{t}^{V0}$ uniformly since infinite cylinders only differ from infinitely prolate spheroids by negligible terms (see [37,55,67]). According to the RT/IRT method, these local and mean operators are weighted averages of the elementary operators $\mathbf{t}^{P}(\boldsymbol{\omega})$, making use, respectively, of the local (for $\mathbf{r} \in Vi \subset V$, resp. for $\mathbf{r} \notin V$) and mean weight functions in V which read:

$$\psi_V(\boldsymbol{\omega}, \mathbf{r}) = -\frac{1}{8\pi^2}\sum_{i=1}^{n} s_{Vi''}(z, \boldsymbol{\omega}), \tag{9a}$$

$$\overline{\psi_V}(\boldsymbol{\omega}) = -\int_{d_V^-(\boldsymbol{\omega})}^{d_V^+(\boldsymbol{\omega})} \left(\sum_{i=1}^{n}\sum_{j=1}^{n} \frac{s_{Vi''}(z, \boldsymbol{\omega}) s_{Vj}(z, \boldsymbol{\omega})}{8\pi^2 v}\right) \mathrm{d}z = \int_{d_V^-(\boldsymbol{\omega})}^{d_V^+(\boldsymbol{\omega})} \left(\sum_{i=1}^{n}\sum_{j=1}^{n} \frac{s_{Vi'}(z, \boldsymbol{\omega}) s_{Vj'}(z, \boldsymbol{\omega})}{8\pi^2 v}\right) \mathrm{d}z, \tag{9b}$$

In Eq. (9b), $\left\lfloor d_V^-(\boldsymbol{\omega}), d_V^+(\boldsymbol{\omega}) \right\rfloor$ is the breadth of the convex hull of the inclusion pattern with support function $d_V(\boldsymbol{\omega})$. It was pointed in [56] that while isotropic distributions have the effect of reducing the interaction, alignments are likely to reinforce it. Patterns of aligned identical inclusions, like spheres or axially symmetric spheroids as well as planar alignments of parallel cylinders, are expected to exhibit the highest pair interaction contributions. We examine planar alignments of equidistant parallel infinite cylindrical cylinders of same radius, and the overall operator variation with their number n and their (assumed common) inter-distance.

3.2 Mean operator of a planar alignment of n cylinders

For identical cylinders planarly aligned in the $x_2{-}x_3$ plane, we denote $\rho_i = \frac{R}{L_i} = \frac{R}{iL} = \frac{\rho_0}{i} \leq \frac{1}{i}$ (with $\rho_0 = R/L$) for the ith neighbor of a reference cylinder $V1$. By extending to n parallel cylinders in this same plane of $x1$ normal the obtained relations for a cylinder pair in Eq. (6), the mean global operator for such a n-alignment reads:

$$\begin{aligned}\overline{\mathbf{t}_{\rho 0}^{\mathrm{ncyl}}} &= \frac{1}{n}\left(n\mathbf{t}^{\mathrm{cyl}} + 2\sum_{i=1}^{n-1}(n-i)\,\overline{\mathbf{t}_{\rho i}^{\mathrm{cyl-cyl}}}\right) \quad = \quad \mathbf{t}^{\mathrm{cyl}} + 2\sum_{i=1}^{n-1}\frac{(n-i)}{n}\left(\frac{\mathbf{v}0}{i^2}\rho_0^2 + \frac{\mathbf{w}0}{i^4}\rho_0^4\right), \\ &= \mathbf{t}^{\mathrm{cyl}} + 2\left(\sigma_2^{(n)}\mathbf{v}0\rho_0^2 + \sigma_4^{(n)}\mathbf{w}0\rho_0^4\right) = \mathbf{t}^{\mathrm{cyl}} + \left(\mathbf{v}0^{(n)}\rho_0^2 + \mathbf{w}0^{(n)}\rho_0^4\right).\end{aligned} \tag{10a}$$

For $n = 2$, $i = 1$, $\sigma_2^{(2)} = \sigma_4^{(2)} = 0.5$ and $\overline{\mathbf{t}_{\rho 0}^{2\mathrm{cyl}}} = \mathbf{t}^{\mathrm{cyl}} + \left(\mathbf{v}0\rho_0^2 + \mathbf{w}0\rho_0^4\right)$, where the $\mathbf{v}0 = \mathbf{v}0^{(2)}$ and $\mathbf{w}0 = \mathbf{w}0^{(2)}$ tensorial notations represent the coefficients of the different nonzero terms as they appear in Table 1. The factors $\sigma_2^{(n)}$ and $\sigma_4^{(n)}$ explicate the evolution of the quadratic and quartic contributions to the interaction operator with the number n of fibers in the alignment. For $n \to \infty$, the limit for the infinite series, $\Sigma(q) = \lim_{n\to\infty}\sigma_q^{(n)} = \lim_{n\to\infty}\sum_{i=1}^{n-1}\frac{(n-i)}{n}\left(\frac{\mathbf{1}}{i^q}\right)$ is the Riemann Zeta function $Z(q) = \lim_{n\to\infty}\sum_{i=1}^{n-1}\left(\frac{\mathbf{1}}{i^q}\right)$, which is finite, $\forall q > 1$.[8] In particular, $Z(2) = \pi^2/6$ and $Z(4) = \pi^4/90$. As defined from the pair interaction as $\mathbf{v}0^{(2)} = 2\sigma_2^{(2)}\mathbf{v}0$ and $\mathbf{w}0^{(2)} = 2\sigma_4^{(2)}\mathbf{w}0$, for a n-planar alignment $\mathbf{v}0^{(2)}$ and $\mathbf{w}0^{(2)}$ are substituted with $\mathbf{v}0^{(n)} = 2\sigma_2^{(n)}\mathbf{v}0^{(2)}$ and $\mathbf{w}0^{(n)} = 2\sigma_4^{(n)}\mathbf{w}0^{(2)}$. With $\sigma_2^{(\infty)} = Z(2) = \pi^2/6$ and $\sigma_4^{(\infty)} = Z(4) = \pi^4/90$, from Eqs. (8) and (10a), at the limit of an infinite alignment of parallel infinite cylinders, one obtains:

$$\overline{\mathbf{t}_{\rho 0}^{\infty\mathrm{cyl}}} = \mathbf{t}^{\mathrm{cyl}} + \left(\mathbf{v}0^{(\infty)}\rho_0^2 + \mathbf{w}0^{(\infty)}\rho_0^4\right) = \mathbf{t}^{\mathrm{cyl}} + 2\left(Z(2)\mathbf{v}0\rho_0^2 + Z(4)\mathbf{w}0\rho_0^4\right), \tag{10b}$$

and with the particular (not always the maximal) values when all the cylinders are at contact:

$$\overline{\mathbf{t}_{\rho 0=1}^{\infty\mathrm{cyl}}} = \mathbf{t}^{\mathrm{cyl}} + 2\left(Z(2)\mathbf{v}0 + Z(4)\mathbf{w}0\right). \tag{10c}$$

Equation (10)a, b, c is exact closed forms that are provided by the IRT method for (a) a n-alignment with general L/R relative inter-distance and (b,c) for an infinite alignment, respectively, at general L/R ratio or at contact ($L = R$), of equally distant cylinders. Owing to the values of $2Z(2) = \pi^2/3 \approx 3,29$ and $2Z(4) = \pi^4/45 \approx 2,16$, it is noteworthy that the global interaction contribution in such an infinite alignment is pretty much more than the interaction contribution from the neighboring first inclusion pairs for the same relative distance ρ_0, $\forall\rho_0 \leq 1$.

Conversely, it is useful to see that for large enough alignments of finite n number of fibers, it is possible to use the operator of the infinite limit: the critical fiber number above which the infinite operator holds depends

[8] The Zeta function has the integral form $Z(q) = \frac{\mathbf{1}}{(q-1)!}\int_0^\infty \frac{x^q}{e^x-1}\mathrm{d}x$.

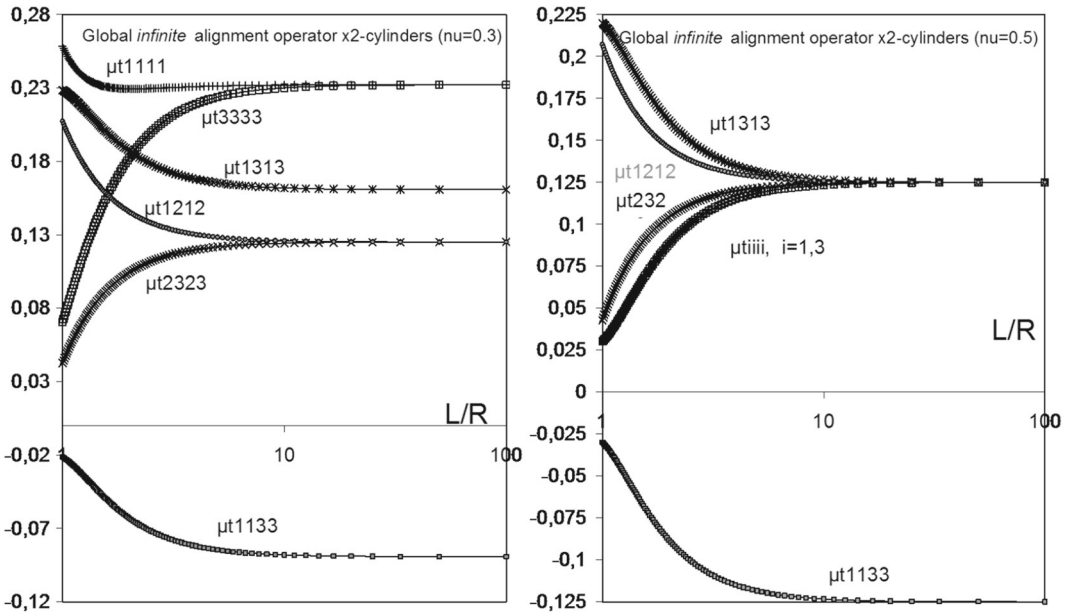

Fig. 4 Global (interior plus interaction) operator for an infinite planar alignment of parallel infinite $x2$-cylinders in plane of normal $x1$

on the inter-distance between fibers and increases when ρ_0 approaches its maximum. It also depends on the desired accuracy for any specific application. For example, the total of the interaction operators farther than $L \geq 10R$ contributes at most (for a compact infinite alignment) by, say, only a few percent to the global one. The evolution of the terms of the pair interaction operator with ρ_0 provides the influence (or cutoff interaction) distance between two fibers above which the interaction can be considered as vanished. For isotropic matrices, this distance depends on the matrix Poisson ratio but not on the shear modulus. It is 2D isotropic around a cylindrical fiber but other fiber cross section shapes are similarly responsible for a 2D anisotropic cutoff interaction distance (not to be examined further here). All these results are similar to those reported in [36] for axial alignments of spheres, in which case the dependency of the pattern operator with the sphere inter-distance ρ_0 involved terms of power 3 and 5 as recalled in Table 1, and the zeta functions $Z(3)$ and $Z(5)$ instead of the terms of power 2 and 4 with the zeta functions $Z(2)$ and $Z(4)$ here obtained in Eq. (10)a, b, c.

It is noteworthy that the operator for an infinite alignment can be used for any finite alignment the total extension of which exceeds the influence or cutoff interaction distance, independently of the fiber number n in it. This conversely indicates that the dilute approximation without interactions strictly holds if a single fiber is isolated in this influence volume, what is of the order of only one percent volume fraction. (This is a maximal effect compared to vanishing average interactions in spatial arrangement of high symmetry, as discussed in [56].)

For elasticity, Fig. 4 reports the global (interior plus interaction) operator as a function of the normalized distance L/R, for the values $\nu = 0,3$ and $\nu = 0,5$ of the Poisson coefficient, in the case of an infinite planar alignment of parallel cylindrical fibers. As for a pair of fibers, at large enough distance L/R between neighboring pairs, the interaction part vanishes and the critical inter-distance for vanishing interaction seems only slightly increased and basically, the influence or cutoff interaction distance does not increase much above the one obtained for the pair interaction operator. (This remark of course depends on the result accuracy one wishes to reach.) More striking is the cumulated interaction amount for an array that concentrates up to make an infinite alignment at contact: in this case, the interaction part is almost equal to the interior one and is capable for, according to the operator component, either duplicate the interior value or cancel it. This clearly means that only considering a single pair interaction (Fig. 3) to represent interactions in a non-dilute concentration of inclusions (here fibers) in a medium is far from accounting for the global interaction contribution (Fig. 4).

The significantly acting elements of the patterns are those interior to this influence distance around one fiber and their number is the ratio of this influence distance to the fiber inter-distance: taking, for example, the influence distance as equal to a dozen of fiber radii (a number which captures more than 90% of the maximum of interaction part an infinite pattern would provide to the global operator), when the fiber inverse inter-distance

ρ_0 increases as $\frac{1}{12}, \frac{1}{6}, \frac{1}{4}, \frac{1}{3}, \frac{1}{2}, 1$ up to contact, the pattern size in the influence zone is, respectively, of 1, 2, 3, 4, 6 and 12 fibers. Using the infinite operator automatically accounts for this variation of pattern size when ρ_0 evolves.

The exemplified alignment of $x2$-oriented fibers being in the plane of normal $x1$, it is possible to check the consistency of the obtained operators from the contact limit case of an infinite alignment: if the fibers were of same square or rectangular cross section (as considered in [57]), their compact alignment would look like a laminate layer, the Green operator of which is well known to have nonzero components $t_{1212} = t_{3232} = B/4$ and $t_{1111} = A + B$, the latter one reaching zero at the incompressible limit ($A = -B$). It is easily verified that for the compact alignment of cylinders the obtained components for the pattern operator evolve similarly with decreasing inter-distance, say toward (although not reaching) zero, except for t_{1212} and t_{1313} which increase and for t_{1111} which either increases or decreases, depending on the matrix compressibility (the Poisson ratio value). The obtained planar pattern operator for fibers in the $x2$ direction also holds for any general (θ, ϕ) orientation, provided the appropriate rotation, as in particular for a general fiber orientation θ in the $x2$–$x3$ plane. For $x3$-oriented fibers it simply results from the appropriate permutation of axes $x2$ and $x3$ in all the pattern operator terms, corresponding to a rotation from $\theta = \pi/2$ to $\theta = 0$.

As is seen from what precedes, a planar layer of parallel equidistant cylindrical fibers needs six parameters (four information) for being geometrically characterized: the number n of parallel elements, the inter-distance $L = R/\rho_0$ between neighboring pairs and two directions $\omega_i = (\theta_i, \phi_i)$ and $\omega_j = (\theta_j, \phi_j)$ for, respectively, the fiber direction and the normal to the fiber layers. When all planar alignments are taken as infinite, any one of them can be specified by only 3 information $(\omega_i, \omega_j, \rho_0) = ((\theta, \phi)_i, (\theta, \phi)_j, \rho_0)$, say 5 parameters, with angles (θ,ϕ), to be explicated when necessary, as exemplified in the next section.

4 Application to effective property estimates for a soft matrix reinforced by a fiber network

We exemplify simple cases of a matrix embedding fiber bundles or networks where planar alignments can be identified as constitutive elements such as to make use of the global fiber pattern operators obtained in the previous sections for determining effective property estimates. As far as one considers a homogeneous medium embedding one, or several other, phase(s) under the form of inclusions or inclusion patterns, in random manner, using the mean field two-point statistics approximation introduced in [34] allows to estimating effective properties in accounting for each phase volume fraction, properties and representative domain shape as well as for some global anisotropy of the spatial distribution symmetry of these phases when possible [68]. The cases of embedded elements that remain co-continuous with the matrix enter this framework as limit cases, typically represented by fibered and layered systems [5,6]. Considering elastic-like or dielectric-like properties, this here on called "PC-W" estimate from [34], for n included phases in matrix with properties $\boldsymbol{C}^M$, takes the generic form:

$$\boldsymbol{C}^{\mathrm{nVi/SDist}}_{\mathrm{effPCW}} = \boldsymbol{C}^M - \left(\left(\sum\nolimits_{i=1}^{n} \left(f_i \left(\left(\boldsymbol{C}^M - \boldsymbol{C}^i \right)^{-1} - \boldsymbol{t}^{Vi}_{\boldsymbol{C}^M} \right) \right)^{-1} \right)^{-1} + \boldsymbol{t}^{\mathrm{SDist.}}_{\boldsymbol{C}^M} \right)^{-1} . \tag{11}$$

In Eq. (11), $\boldsymbol{t}^{Vi}_{\boldsymbol{C}^M}$ is the mean operator of the representative domain Vi for phase i (a single inclusion of phase i, or a finite pattern of them) having $\boldsymbol{C}^i$ properties and f_i volume fraction and $\boldsymbol{t}^{\mathrm{SDist.}}_{\boldsymbol{C}^M}$ is the (formally ellipsoidal) operator representing some common spatial distribution symmetry for all the Vi domains in the matrix. This distribution symmetry operator can also be seen as the operator of the representative (ellipsoidal) elementary matrix volume V_M containing the pattern Vi. This latter understanding fixes a concentration limit for the validity of the PC-W estimate, related to the minimal reference volume size capable of containing the representative patterns of the embedded phases, in the sense of an (ellipsoidal) envelop of these patterns [34,35]. When the domains Vi are single inclusions, the PC-W estimate statistically accounts for a part of their interactions through their spatial distribution, but the larger are the chosen representative patterns Vi, the more precisely the pair interactions can be accounted for at the pattern scale.[9] As far as the considered patterns are finite sets, the estimate still regards the pair interactions between any two patterns through their spatial distribution and the dilute approximation that characterizes this estimate type still applies at the pattern

[9] Patterns with mixed inclusion pair interactions, not accounted for in Eq. (11), appear in [65].

scale. Equation (11) will be enough for the following discussion purpose about the use of infinite patterns, and especially the two-phase form of it (a unique embedded phase) which simplifies to:

$$\boldsymbol{C}^{\mathrm{V/SDist}}_{\mathrm{effPCW}} = \boldsymbol{C}^{M} - f_V \left(\left(\left(\boldsymbol{C}^{M} - \boldsymbol{C}^{V} \right)^{-1} - \boldsymbol{t}^{V}_{\boldsymbol{C}^{M}} \right) + f_V \boldsymbol{t}^{\mathrm{SDist.}}_{\boldsymbol{C}^{M}} \right)^{-1} . \tag{12}$$

In Eq. (12), the embedded phase has volume fraction $f_V = 1 - f_M$ and properties $\boldsymbol{C}^V$, a representative inclusion or pattern V with mean global operator $\boldsymbol{t}^{V}_{\boldsymbol{C}^M}$, and these patterns are spatially distributed according to some (ellipsoidal) symmetry represented by the operator $\boldsymbol{t}^{\mathrm{SDist.}}_{\boldsymbol{C}^M}$. Assuming statistical homogeneity of the individual elements, regardless of the pattern, f_V must also be the inclusion concentration in the pattern, say the volume fraction of V in its elementary matrix volume V_M (a difference would represent some inclusion clustering in the patterns, the statistical homogeneity assumption applying then at the pattern distribution scale).

Now, when a composite comprises a compliant matrix and a stiffer embedded phase, the inclusion arrangement inside the representative pattern is expected to evolve with the matrix deformation (changes of the inclusion shape being considered as negligible in comparison), this expectedly having an effect on the pattern element interactions. The description of such evolutions can be simplified when global operators for typical large (infinite-like) inclusion patterns are available in closed form, as those for aligned spheres and spheroids [36], for coaxial finite cylinders [37] and for planar arrays of infinite fibers (this present work) to which we here pay special attention.

In what follows we only consider changes of the material two-phase microstructure (whether them coming directly from the elaboration process or from some applied deformation on an initial microstructure) for which everything but the fiber arrangement remains invariant and the individual fibers can be assumed to: (1) not deform (they remain straight and of fixed circular cross section) and (2) all remain parallel to a same direction (that may vary) by definition of a 1D bundle. That is we disregard all situations of possible bending, flexion and torsion modes for the fibers or for their arrays, to which a separate analysis needs to be dedicated. We furthermore disregard any interface de-cohesion between the fibers and the embedding matrix which is assumed compliant enough for so doing if the microstructural changes result from some applied mechanical loading.

The focus is on the examination of estimated variations of effective property estimates when (no matter so much how) changes occur, in the above-specified limits, in a representative volume element (RVE) of the fiber arrangement. We compare estimates resulting from different possible descriptions of this fiber arrangement, paying special attention to descriptions making use of infinite patterns in some simple/simplified way for easy use, in comparison with more commonly used simpler finite patterns. Comparisons with experiments are also let out of the present scope, except some numerical ones to provide some comparison data. It is worth to here specify that comparisons with any finite element numerical simulation data can only capture tendencies (not accurate match), owing to the impossibility of describing similarly the boundary conditions and the material microstructural features as in homogenization framework (infinite matrix, isotropic inclusion or fiber arrangements, etc.).

The first selected example is simple matrix reinforcement by a one-directional (1D) fiber bundle, characterized by a regular arrangement of parallel infinite cylindrical fibers of same radius R as viewed from a bundle cross section. More complex networks can often be described as several interpenetrated bundles of parallel cylindrical fibers from this one-directional type. And these structures can be seen in different manners as arrangements of interpenetrated layers of infinite planar patterns. One-directional cylinder bundles represent the basic simplest form of more general fiber bundles or networks possibly also involving fibers of non- circular section shape. We here only consider cylindrical fibers; rectangular beams have been addressed in [57] in a different context but in a similar (planar alignment) manner.

4.1 Description of 1D fiber-reinforced matrices from infinite planar arrays of infinite fibers

A one-directional bundle of parallel fibers can be described in different manners, as exemplified in Fig. 5, by cross section views of normal $\omega_i = (\theta_i, \phi_i)$. On the left side example, the fibers are taken as randomly distributed in isotropic manner (no spatial arrangement is accounted for if any) with ignored specific pair interactions what means a validity restriction to “dilute enough concentrations”.

The representative volume element (RVE) is a matrix cylinder embedding a single fiber and straining such a material amounts to modify this RVE (whose shape represents the spatial fiber distribution) from isotropic to

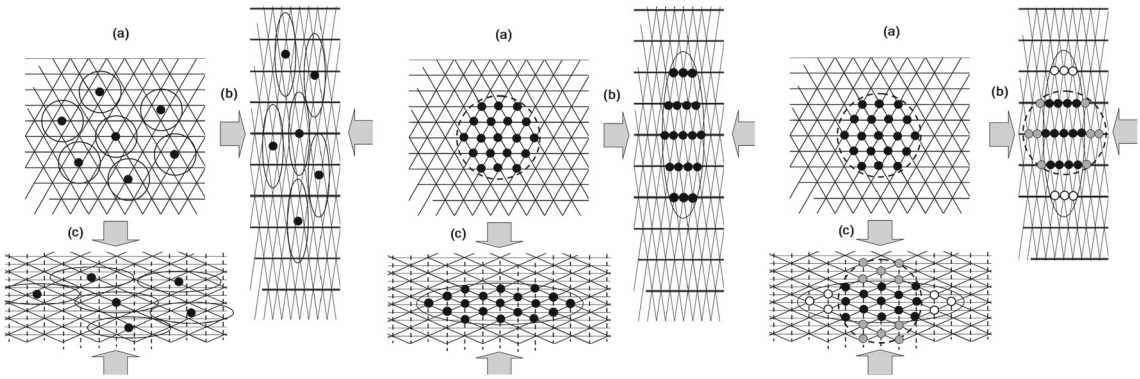

Fig. 5 2D isotropic (**a**) and horizontally (**b**) or vertically (**c**) strained elementary volume of 1D fiber-reinforced matrix using a RVE comprising, from left to right : a single fiber, a finite fiber pattern and the finite part of an infinite fiber pattern contained in a (2D isotropic) influence zone

elliptic according to a direction of compression- or extension-like stretch. In the central description, a regularly enough arrangement of the fibers which are aligned and with nearly equal inter-distances in parallel planes is taken into account with using a finite pattern representative of the major interactions between fibers in the bundle.

A minimum of 3 or 4 fibers is representative of the first-neighbors interactions and larger sets can be selected as well, the more complex the pattern and the pairs interactions inside it when the larger is the fiber number. If substituting a finite pattern to a unique fiber allows accounting for interaction within the chosen pattern, pair interactions between patterns remain only accounted for through their spatial distribution. Such a description holds for dilute enough concentrations of the selected pattern unless it is large enough to attain the size of the influence domain, above which case it becomes simpler to consider an infinite pattern. A major advantage is that while finite patterns cannot be valid for any fiber volume fraction in the matrix to follow a possibly evolving fiber arrangement when smaller than the influence zone, using an infinite pattern has open validity range. And while for any finite pattern not reaching the influence domain size it is still necessary to attribute it a matrix volume that varies in shape accordingly with the fiber pattern, above this influence size the shape of the reference matrix domain becomes the one of the influence domain shape itself which is not varying with the pattern arrangement. The changes of the pattern part inside this domain are those which matter for the effective properties to be estimated.

This corresponds to the third right-hand-side example of Fig. 5, where the pattern is assumed being infinite with only a finite part of it contributing to the interaction estimate due to the finite interaction or influence distance represented by the dotted circle, with possibly entering new (gray) elements and possibly getting out other (white) ones during a deformation-like change in the fiber arrangement. Whether the pattern of several fibers is finite or infinite, the fiber concentration limit is given by the arrangement at which fibers become in contact, since they cannot overlap each other. Further evolutions will depend on the allowed fiber rearrangement possibilities inside the matrix, what is not in the present scope. For cylinders of same radius, the compact regular (hexagonal) piling corresponds to a concentration $f_{\max} = \pi/2\sqrt{3} \approx 0{,}906$. This concentration limit is further decreased when the fibers are not in hexagonal piling, as described next.

As far as in the bundle the fibers can be assumed regularly enough arranged such as to appear aligned and with nearly equal inter-distances in parallel planes, these planar alignments are characterized by the fiber inter-distance and an ω_j-oriented normal around the ω_i fiber axis. Thus, such fiber arrangements around any selected fiber can be fully represented by an appropriately weighted average $\langle . \rangle_{\omega j}$ over a set of orientations ω_j around the ω_i axis of the layer operators $\boldsymbol{t}_{\boldsymbol{C}^M}^{\infty \mathrm{Fib}(\omega_i,\omega_j,\rho 0)}$, what provides a global bundle operator $\boldsymbol{t}_{\boldsymbol{C}^M}^{\infty \mathrm{Fib}\langle \omega_i,\rho 0_i\rangle_{\omega j}}$. This can be approximated in only considering the few densest planar arrays of fibers that well enough represent the bundle. As shown in Fig. 5 right, this bundle representation needs properly describe elements entering the cutoff interaction distance (the gray ones) as well as those getting out of it (the white ones) when the fiber arrangement changes. Also, the main and densest planar arrays do not necessarily remain invariant, as visible in Fig. 5c right where the vertical array (dotted parallel lines) becomes denser than the horizontal one.

Rather than calculating all pair interactions inside such a bundle (what is possible), it can be simplifying to making use of the main operators for the infinite planar arrays representative of the bundle for the follow-up

of fiber arrangement evolutions or changes in it. The global operator for such an infinite bundle, $\boldsymbol{t}_{\boldsymbol{C}^M}^{\infty\mathrm{Fib}\langle\omega_i,\rho 0_i\rangle_{\omega j}}$ say, can thus be obtained from appropriately summing all or the main constitutive infinite planar alignments around their common fiber direction.

Using the PC-W estimate with considering nearly 1D bundles of infinite circular fibers organized according to a 2D isotropic influence zone yields effective properties of the form:

$$\boldsymbol{C}_{\mathrm{effPCW}}^{\infty\mathrm{Fib}\langle\omega_i,\rho 0_i\rangle_{\omega j}} = \boldsymbol{C}^M - f_F\left(\left(\boldsymbol{C}^M - C^F\right)^{-1} - \boldsymbol{t}_{\boldsymbol{C}^M}^{\infty\mathrm{Fib}\langle\omega_i,\rho 0_i\rangle_{\omega j}} + f_F\boldsymbol{t}_{\boldsymbol{C}^M}^{\mathrm{SDist.}}\right)^{-1}. \tag{13}$$

It is without loss of generality that the efficiency of such a global infinite bundle operator $\boldsymbol{t}_{\boldsymbol{C}^M}^{\infty\mathrm{Fib}\langle\omega_i,\rho 0_i\rangle_{\omega j}}$ can be examined with simply considering the 3 or 4 main layer orientations generally having different inter-distances $L_j = R/\rho_j$. As will be exemplified next on, appropriate average of these main planar pattern operators describing the bundle arrangement is likely sufficient to provide a quite simple reasonable approximation for $\boldsymbol{t}_{\boldsymbol{C}^M}^{\infty\mathrm{Fib}\langle\omega_i,\rho 0_i\rangle_{\omega j}}$, owing to the simple operator form for planar arrays and from it in Eq. (13), effective property estimates to compares with more classical ones using no or finite small fiber patterns.

If the changes in the bundle fiber arrangement in the composite are assumed to be the results of a homogeneous strain of the matrix (normally to the fiber direction), the variation of this characteristic set of currently densest fiber arrays allows quite easily to varying the pattern operators according to the evolution of the composite structure, in varying their orientations together with varying accordingly the fiber inter-distance in these layers. Comparing effective property differences between different bundle fiber arrangements directly resulting from elaboration will follow the same procedure.

In order to simplify the discussion and to simply image the points in concern, we make use of the deformation-like origin for the changes in the bundle fiber arrangement and both fiber and matrix phases will be considered as incompressible while deformation in the infinite fiber direction will be disregarded. This allows assuming a constant area for the cross section of any bundle RVE. Starting from the regular hexagonal arrangement that may be seen as the undeformed reference one with corresponding to a $\eta = 1$ "stretch factor" (Fig. 5a, middle and right), any change of this η value can be seen as a tensile or compressive stretch normally to the fiber direction taken along the $x3$ axis or $x1$ axis as shown in Fig. 5b, c. It is worth pointing at first that the two ranges $\eta > 1$ and $\eta < 1$ do not correspond to symmetric changes of the fiber arrangement in the matrix: according to the drawings of a first-neighbors pattern in Fig. 6, a stretch $\eta > 1$ along $x3$ extends the initial reference equilateral triangle of Fig. 6 left for $\eta = 1$ into the one of Fig. 6 middle, while the converse stretch $\eta < 1$ along $x3$ first yields to a square arrangement as shown in Fig. 6c at $\eta = \eta_0 = 1/\sqrt{3}$. For η values lower than $\eta_0 = 1/\sqrt{3}$, the fiber arrangement evolves as for $\eta > 1$ up to a $\pi/2$ rotation. A $\pi/2$ rotated hexagonal arrangement is retrieved at $\eta = 1/3$, and any $\eta = k > 1$ value has a $\pi/2$ rotated equivalent at $\eta = 1/3k$ with a $k_{\max}$ limit when the fibers get into contact in the densest of the planes in the pattern (when $\eta < 1/3$, the horizontal alignments become the densest ones in place of the vertical alignments when $\eta > 1$). Owing to this

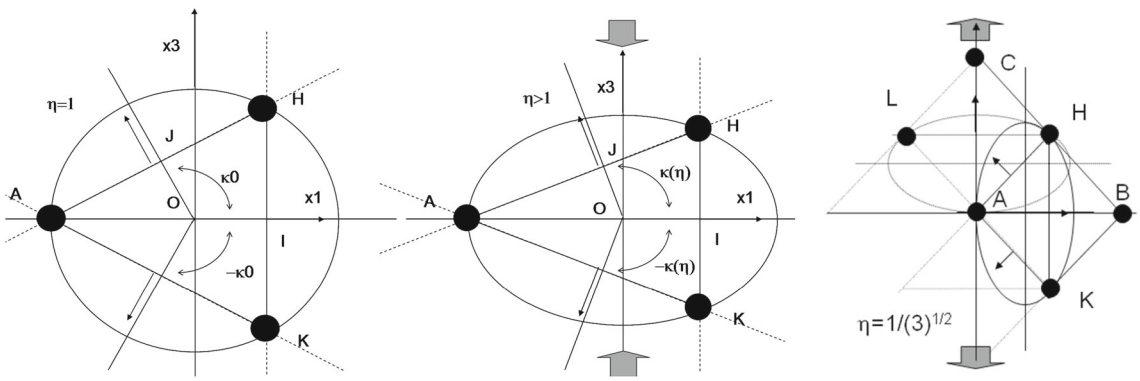

Fig. 6 A 3-element minimal cylinder pattern, for (left) a regular hexagonal array, $\eta = 1$; (middle) a compressed-like array along $x3$ axis for $\eta > 1$, for constant area cross section (the related 3 main infinite alignments—dashed lines—represent the corresponding infinite pattern); (right) the 4-element (losange AHBK) pattern in the $x3$ extended-like square arrangement for $\eta = 1/\sqrt{3}$.

symmetry, we have explored the half range $\eta > 1/\sqrt{3}$, using the four planes of the losange 4-fiber pattern that needs to be accounted for in the square arrangement at $\eta = 1/\sqrt{3}$, as shown in Fig. 6 right.

The evolution (or variation) of this pattern can be described as follows: the matrix is considered as almost incompressible and the area of the elliptic disk is assumed to remain constant ($\pi R^2 = \pi ab = \pi b^2 \eta = \pi a^2/\eta$) where $a = OA$ and b is the second ellipse semi-axis. The alignment of normal $x1$ (resp. $x3$) keeps the φ angle to 0 (resp. $\pi/2$), while for the two other ones, $\kappa 0$ evolves—in the considered η range—from $\pm 2\pi/3$ to $\pm\left((\pi/2) + \tan^{-1}(1/\eta\sqrt{3})\right)$. The fiber inter-distances, respectively, vary as $\frac{HK_\eta}{HK_1} = \frac{1}{\sqrt{\eta}}$ for the vertical alignments, $\frac{AI_\eta}{AI_1} = \sqrt{\eta}$ for the horizontal ones and $\frac{AH_\eta}{AH_1} = \frac{AK_\eta}{AK_1} = \frac{\sqrt{3\eta+(1/\eta)}}{2}$ for the two types of oblique ones. When $\eta = 1$, 3 fiber inter-distances are equal on the vertical and oblique alignments such that $IH_1 = L_1$ and the concentration of fibers (with radius r) reads $f = \frac{0.5\pi r^2}{L_1^2\sqrt{3}} = \frac{0.5\pi L_1^2 \rho^2}{L_1^2\sqrt{3}} = \frac{\pi\rho^2}{2\sqrt{3}} = f_{\max}\rho^2 \leq f_{\max}$. For $\eta > 1$, the first fiber contact limit is in the vertical alignments for which the inter-distance is the smaller, such that $IH_\eta = L_\eta = L_1/\sqrt{\eta}$ provides the new first contact limit. The fiber volume fraction at this contact when η increases corresponds to $\rho_\eta = r/L_\eta = \sqrt{\eta}\,(r/L_1) = \rho\sqrt{\eta}$, with the limit being at $\rho_\eta = 1$, thus $\lim(\rho^2) = \lim(\rho_\eta^2/\eta) = 1/\eta$ say $f_{\lim} = \frac{\pi}{2\sqrt{3}}\frac{1}{\eta} = \frac{f_{\max}}{\eta}$. For the square arrangement (decreasing η to $1/\sqrt{3}$) the maximal fiber concentration is for fibers at contact along the oblique planes where $\rho_\eta = \frac{r}{L_\eta} = \frac{2}{\sqrt{3\eta+(1/\eta)}}\frac{r}{L_1} = \frac{2\rho}{\sqrt{3\eta+(1/\eta)}}$, $\lim(\rho^2) = \lim\left({\rho^2}_\eta \frac{3\eta+(1/\eta)}{4}\right) = \frac{3\eta+(1/\eta)}{4}$, say $f_{\lim} = f_{\max}\frac{3\eta+(1/\eta)}{4}$, equal to $f_{\lim} = \frac{\pi}{4}$ at $\eta = 1/\sqrt{3}$.

4.2 Estimates of effective properties of 1D fiber-reinforced matrices

Based on the three structure descriptions shown in Fig. 5 for a 1D fiber bundle for some different spatial arrangement of the fibers, we compare the corresponding estimates of effective properties, using the generic Eq. (13) for the three of them, in the case of a matrix straining-like that corresponds to a fiber arrangement change as for a vertical compressive mode):

- For the representative volume with a single fiber in elliptic description with aspect ratio $\eta > 1$ (Fig. 5, left), the elliptic distribution operator is given in Table 1 column1, which also gives the cylindrical fiber operator when taking $\eta = 1$;
- For the middle case of Fig. 5, the same η-elliptic fiber operator describes the finite pattern distribution, while the pattern mean operator is the sum of the pair interaction operators in the considered pattern, according to (8)–(10). We assume the elementary finite pattern to have the same "elliptic" symmetry (η) as the distribution operator, taken to correspond with planes, the normal of which are at angles κ as defined in Fig. 6. This pattern, when reduced to its minimum to hold for any η value on both sides of the square symmetric pattern at $\eta = \eta_0 = 1/\sqrt{3}$, needs the fourfold set of main (densest) fiber planar alignments (twice the triangle of Fig. 6a,b, symmetrically duplicated into a losange that yields the square pattern in Fig. 6c) specified by the 4 inter-distances and the 4 plane orientations as described in the previous section. Each of these four constitutive main alignments can be considered made of a same number of n elements, with n ranging from 2 to any value that makes the distance between two extreme fibers larger than the cutoff interaction (influence) distance, even in the case the n fibers are at contact. According to the here estimated influence distance, n should be larger than the ten to twenty critical number of fibers, n_{critic} say. In this latter case ($n > n_{\text{critic}}$), the interaction terms can be taken as being those of the infinite alignment. We report the data obtained for the two extreme assumptions ($n = 2$ and n "infinite" for $n > n_{\text{critic}}$) that correspond, respectively, to Eqs. (7) and (10b).
- For the third (right hand side) case in Fig. 5 that also makes use of a four infinite alignment pattern, the invariant 2D isotropic distribution is represented by the cylinder operator. Comparing these two estimates that make use of the same infinite pattern but in different distribution symmetries allows to specifically examining the effect of taking that constant distribution symmetry rather than an elliptic one that varies with the pattern.

For the isotropic matrix phase that embeds this fiber bundle, the only elastic property of interest is the Poisson ratio υ^M, while only the relative elastic stiffness moduli of the fibers $\mathbf{C}^F/\mu^M$ are needed, μ^M being the matrix shear modulus. Although $\mathbf{C}^F$ can be taken of general anisotropy, we here consider isotropically

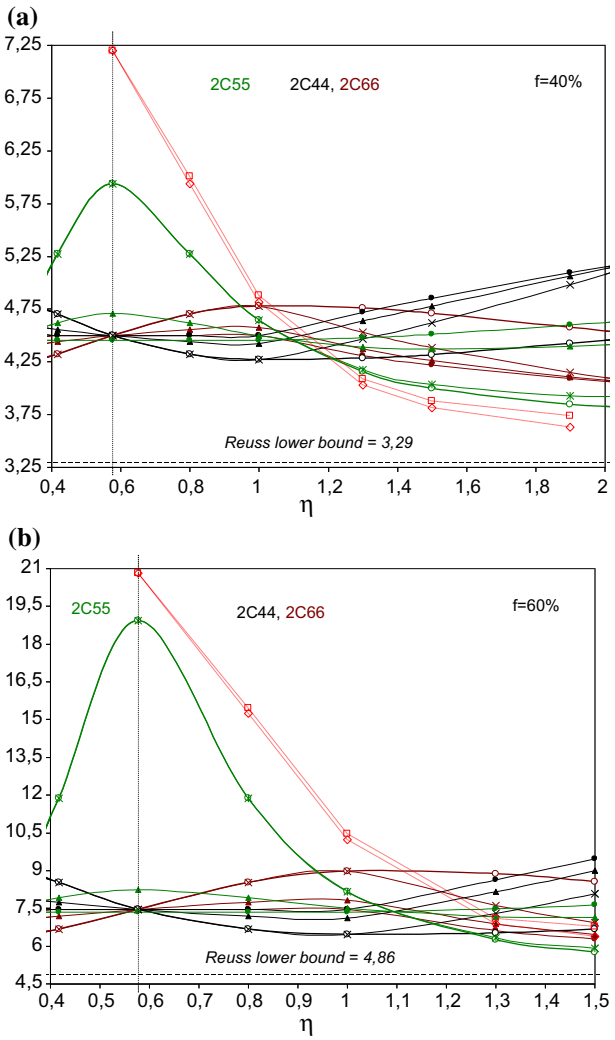

Fig. 7 Evolution with a stretch η of the three effective shear moduli at 40% (**a**) and 60% (**b**) fiber volume fraction from the four compared estimates (single fiber, elementary pattern and $n > n_{\text{critic}}$ -elements in η-elliptic distribution are represented by black dots, triangles and crosses, the infinite pattern in a fixed influence zone by white dots on a bold line). Numerical 2D simulations for the in-plane shear modulus 2C55 reported for comparison are plotted as points linked by dashed straight lines

incompressible elastic fibers for sake of simplicity ($\upsilon^F = 0.499$) and since the matrix is assumed highly compliant in comparison with the fibers, one considers $\mu^F = 50\mu^M$.

We arbitrarily choose $\upsilon^M = 0.49$ for keeping a nearly incompressible matrix. We present and discuss for the four compared different estimates the variations with the fiber arrangement (say with η) of the three effective shear moduli and of the two effective Young moduli transverse to the fibers (the axial Young modulus Y2 being in all cases given by the Voigt upper—arithmetic mean—bound). Except for Y2, all results are on the Reuss lower bound side, as expected for hard inclusions in a soft matrix. From these data which are presented in Figs. 7 and 8, one firstly observe that the 2 estimates based on the use of an infinite pattern to represent (even in a simplified manner) the fiber bundle are markedly different from those which make use of more simpler descriptors of the fiber arrangement, while the two estimates of each pair do not differ much. The few reported comparisons with numerical simulations also clearly evidence that the former pair (infinite alignment pattern) better capture the major features of effective property changes due to the fiber arrangement than the latter ones. Figure 7a, b, respectively, presents for 40 and 60% fiber concentrations, the 3 effective shear moduli variations with η from 0.4 (slightly less than the square symmetric arrangement $1/\sqrt{3} \approx 0.57735$) to nearly the maximal stretch with no fiber contact, for the four compared estimates: it is seen on both figures that while for 2C44 (C_{2323}) and 2C66 (C_{1212}) (which clearly appear to reverse from $\eta > 1/\sqrt{3}$ to $\eta < 1/\sqrt{3}$,

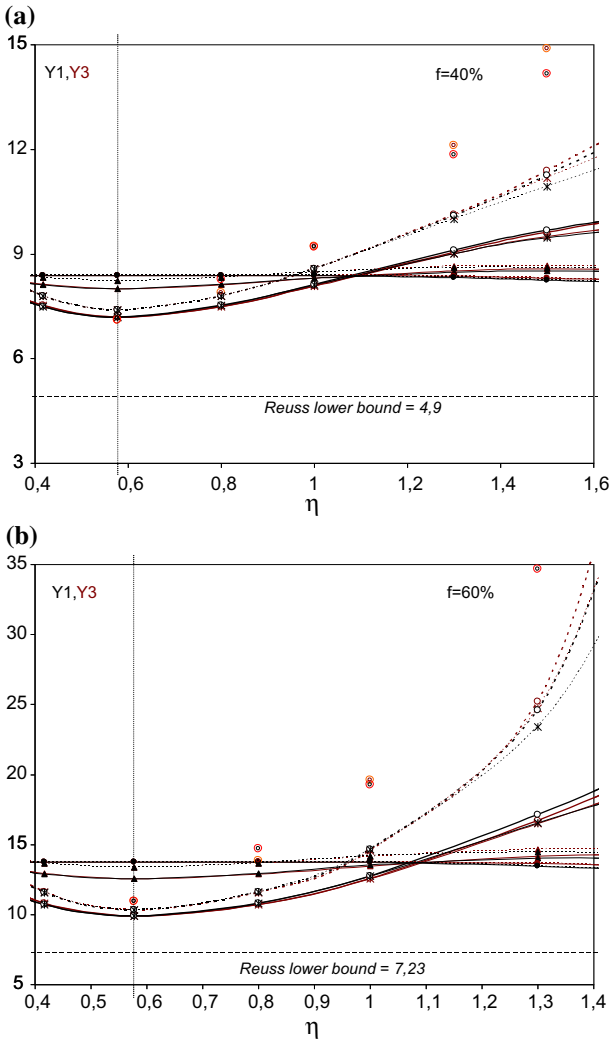

Fig. 8 Evolution with a stretch η of the two transverse effective Young moduli at 40% (**a**) and 60% (**b**) fiber volume fraction from the four compared estimates (single fiber, elementary pattern and $n > n_{\text{critic}}$-elements in η-elliptic distribution are represented by black dots, triangles and crosses, the infinite pattern in a fixed influence zone by white dots on a bold line). Full and dashed lines correspond to two different weight sets given to the four terms patterns taken to represent the bundle in each of the four compared estimates. Numerical 2D simulations are plotted as open double circles for comparison

the square pattern position been indicated by the vertical dotted line) the variation remains moderate, there is a sharp change for the 2C55 (C_{1313}) modulus, in the cross section plane. This is the shear modulus that has been compared with 2D numerical simulations using the bundle RVE and simulation calculation method summarized in "Appendix C". It is quite striking that only the two estimates making use of the infinite planar finer alignments capture the main features of this modulus evolution with η (changes of fiber arrangement) over almost all the explored range. Here, the four main planar alignments have been considered over the whole η range with weights (1/6,1/3,1/3,1/6) since in a losange 4-fiber pattern, the weights of the two oblique planes are twice those of the $x1$ and $x3$ planes as shown in Fig. 6.

Figure 8a, b similarly reports the same estimates for the two transverse Young moduli as well as 2D numerical simulations performed according to "Appendix C" procedure. As for the shear moduli, the estimates that make use of the infinite planar alignments better capture the Young moduli evolutions with η, especially in the range $\eta < 1$ but do not reach the numerically estimated moduli values when η becomes large. These latter values can be overestimated because the matrix meshing becomes difficult when the fibers get close to each other in some of the planar alignments and one can consider the well-reproduced tendency as a satisfying result. Also, since the pattern of 4 main alignments necessarily omits possibly also influent few additional ones, the best weights to be given to the fourfold set may not be (1/6,1/3,1/3,1/6): in order to show this, the set of dotted

lines which get closer to the numerical values correspond to a different weight set that enhances the contribution of the densest plane, namely based on using the function arcsin(R/Li) ($i = 1, 4$, for the four main alignments) in normalized manner,[10] as if each of the four alignments is weighted to also account for complementary alignments in its angular sector. Unfortunately, this alternative weighting (arbitrary) assumption that appears better for the Young moduli becomes less satisfying for the 2C55 shear moduli even if the main tendency as in Fig. 7 is still obtained (not reported for room saving and sake of clarity in the figures). That again means that the estimate improvements may need to account for some more alignments to more accurately describe the bundles, what is a still ongoing analysis not to be entered here. If the proposed simplification of the fiber bundle by a limited set of 3 or 4 main planar alignments turns to appear too-simplified to be valid over the whole possible range of fiber arrangements as represented by the η parameter, it quite well holds for a large η range already. And the obtained results with the proposed simplifications clearly show that the use of infinite alignments appears to significantly improve the obtained moduli estimates compared to more classical estimates with a single fiber or a small pattern of first near neighbors. In that respect, it is noteworthy that, provided all pair interactions being conveniently accounted for in such an infinite pattern description of the fiber arrangement, the resulting mean field estimate will no more be a dilute concentration approximation, being a dilute concentration applying on patterns that are infinite and individually representing the whole fiber arrangement. At last, the weak difference due to whether the reference domain is elliptically varying or constant 2D isotropic shows that considering the invariant influence domain with an infinite bundle is relevant.

As the fiber arrangement is described, the fiber concentration limit is given by the impossible overlapping of any two fibers. If the changes in the composite structure result from a deformation process (as for the given example of compression or extension transversally to the fibers) other processes in the fiber rearrangements need to be described appropriately to allow further deformation beyond the contact limit. And if the fiber arrangement evolution can still be described from planar alignments, the modeling can be pursued with the appropriate representative (infinite and fully interacting) pattern. It is worth insisting on the fact that the reported results also hold for fiber arrangements having some η ellipticity that may simply result from the composite elaboration, and not necessarily from an applied deformation on it.

Now, in the extreme case when the fibers are dense in a single set of parallel planes (of normal ω_j) and with large enough distances between the planes to neglect transverse interactions, the structure can be treated as a laminate structure made of fiber-reinforced layers of matrix with distribution symmetry represented by the platelet operator $\boldsymbol{t}_{\boldsymbol{C}^M}^{p\omega_j}$ (from Table 1, column 1, with $\eta = 0$ or infinite according to the laminate normal orientation $x1$ or $x3$, respectively). A property estimate from the PC-W framework for such a laminate structure reads:

$$\boldsymbol{C}_{\text{effPCW}}^{\infty\text{Fib}(\omega_i,\omega_j,\rho 0_i)} = \boldsymbol{C}^M - f_F \left(\left(\boldsymbol{C}^M - \boldsymbol{C}^F \right)^{-1} - \boldsymbol{t}_{\boldsymbol{C}^M}^{\infty\text{Fib}(\omega_i,\omega_j,\rho 0_i)} + f_F \boldsymbol{t}_{\boldsymbol{C}^M}^{p\omega_j} \right)^{-1}, \tag{14}$$

using the single $\boldsymbol{t}_{\boldsymbol{C}^M}^{\infty\text{Fib}(\omega_i,\omega_j,\rho 0_i)}$ operator for the infinite planar pattern of fibers and for the distribution, the laminate operator $\boldsymbol{t}_{\boldsymbol{C}^M}^{p\omega_j}$ of same normal (from Table 1, column 1 with appropriate η value and rotated orientation).

4.3 Extension to fiber networks as interpenetrated parallel fiber bundles

Now consider a layered structure still made of planarly fiber-reinforced (soft) matrices and issued from a 1D bundle as the one of Fig. 9a (similar to the one of Fig. 5 but with a rectangular rather than hexagonal array of fibers) by alternatively rotating the successive layers along the normal axis $x3$ say, at plus or minus φ (not necessarily orthogonal) angle with regard to the $x1$ axis. This is illustrated in Fig. 9b where the odd and even fiber layers numbered

$$(n_{11}, \ldots, n_{61} \ldots), \left(n_{13}, \ldots, n_{63,\ldots}\right), (n_{15}, \ldots, n_{65}, \ldots), \ldots$$

and

$$(n_{12}, \ldots, n_{62} \ldots), \left(n_{14}, \ldots, n_{64,\ldots}\right), (n_{16}, \ldots, n_{66}, \ldots), \ldots$$

alternate.

[10] Each arcsin(R/Li) function for the four alignments is divided by the sum of them four.

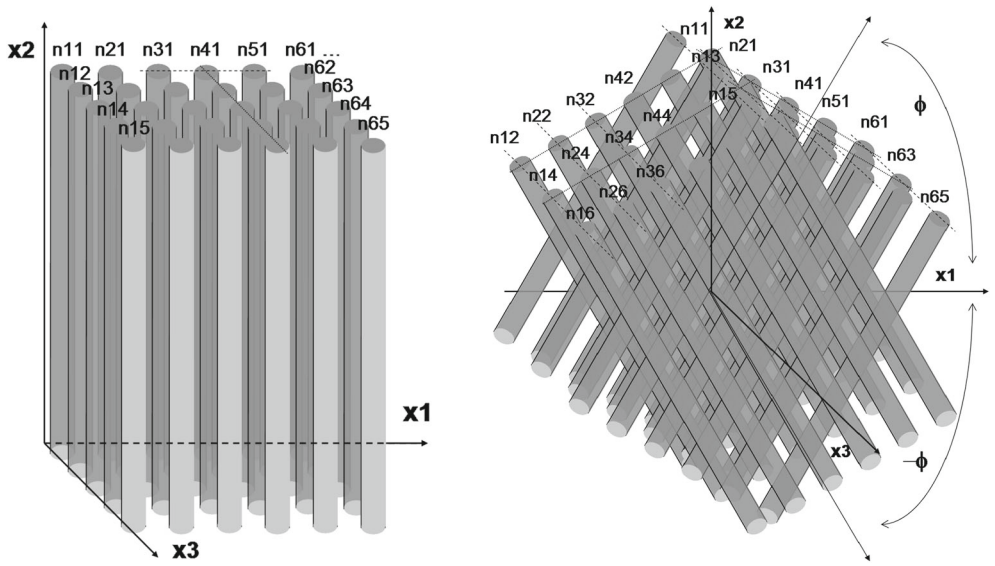

Fig. 9 A one-directional rectangular fiber bundle (a) transformed into a two-directional arrangement of infinite and planarly aligned infinite fibers by alternated layer rotations $(+\varphi, -\varphi)$

The fibers are equidistant in all layers, and the fiber radius R and their inter-distances $L = R/\rho_0$ are also taken identical in the two-layer types, although they may be different more generally. Also assume the layers parallel the $x1$–$x2$ plane to have equal thicknesses or inter-distances such that both layer types contribute to 50% of the composite material.

Under still simple deformation modes and still assuming rigid fibers (neither bending nor torsion allowed), such a structure may not only change the inter-distances between fibers as for the previous 1D bundle (as would result from a compression along $x3$ axis for example) but also reorient the different fiber layers by a change of the angles $\pm\phi$ (under a tension in the $x1$–$x2$ plane for example).

This two-directional arrangement could be reasonably well described as a bilayered laminate structure with $x3$ normal axis and effective properties for such a bilayered structure can be obtained in applying the classical two-phase laminate scheme [20] on the homogeneous two materials equivalent to each layer structure type, which only differ by a 2φ disorientation. The effective properties for the two individual layer types could be estimated by the laminate solution of Eq. (14) with taking the appropriate fiber orientation $\omega_{\pm i} = (\pi/2, \pm\phi)$, according to the φ rotation around the x_3 axis. Yet, so-doing this laminate-based estimate would not take into account the trans-layers fiber interactions and would not be very accurate if the layer thicknesses are to thin (if the alternated layers are too close to each other, say).

This laminate-base estimate is applicable to any number of disoriented interpenetrated bundles larger than two, provided they all are rotated around a same axis, which will be the normal to the layered description. It does not apply when more than two bundles are interpenetrated otherwise, as, for example, a third bundle with $x3$-fiber orientation is introduced in the pattern of Fig. 9 right.

Relevant alternatives for structures that exhibit multi-directional phase co-continuity features consist in using either a fiber system scheme or a laminate system scheme, according to the references [1,2,4–6,32] given in introduction. A property estimate from a fiber system or a laminate system scheme consists in averaging (arithmetically) the property estimates from an elementary 1D fiber or laminate structure over some (possibly discrete) distribution of (fiber or laminate normal) orientations ω_j.

For estimating properties from a laminate system scheme, the elementary 1D laminate structure can assemble as many different parallel phase layers as involved in the composite to be described, in using $\boldsymbol{t}^{Vi}_{\boldsymbol{C}^M} = \boldsymbol{t}^{\mathrm{SDist}}_{\boldsymbol{C}^M} = \boldsymbol{t}^{p\omega_j}_{\boldsymbol{C}^M}$ in Eq. (11), and the reference matrix possibly being any one of the assembled phases. In an elementary 1D laminate structure with normal ω_j, all the involved phases are co-continuous normally to ω_j with Voigt-like effective moduli in this plane while they are, with some modulation according to the modeling details, Reuss-like (harmonic average) in direction ω_j.

For estimating properties from a fiber system scheme, the elementary 1D fiber structure can be described with making use of as many fibers as appropriate in the representative pattern, provided that all are parallel. In

that respect, disregarding the "quality" differences, the effective properties obtained from any one of the four descriptions for the 1D fiber bundle that are compared in Sect. 4.2 (from Eq. (12)) for a two-phase material could be used (parallel fibers of different phases can also appear in the 1D bundle description if more than one phase is embedded) with a better capture of the effective moduli for the estimates that make use of infinite alignments. In a 1D fiber structure, the effective moduli are Voigt-like with regard to the fiber direction ω_j and, also with some modeling-due modulations, are nearly Reuss-like normally to it.

Consequently, laminate system schemes are more appropriate when multi-directional phase co-continuity needs to be accounted for without distinction between the involved phases, while fiber systems are more appropriate if one of the phases plays a specific role (as a matrix). Both become of interest when interpenetrated 1D fiber bundles are to be considered, with the best choice depending on the specific situation.

For the structure exemplified in Fig. 9 right, this fiber arrangement can also be seen (if the fibers are also well aligned in alternatively identical layers) as two interpenetrated arrays of planarly aligned cylinders, with normal oriented at $\pm\phi^* = \pm\left(\frac{\pi}{2} - \phi\right)$, as represented by the layers

$$(n_{12}, n_{14}, n_{16} \ldots)\,, (n_{22}, n_{24}, n_{26} \ldots)\,, (n_{32}, n_{34}, n_{36} \ldots)\,, \ldots$$

and

$$(n_{11}, n_{13}, n_{15} \ldots)\,, (n_{21}, n_{23}, n_{25} \ldots)\,, (n_{31}, n_{33}, n_{35} \ldots)\,, \ldots.$$

A property estimate could then be obtained from using a two-layer laminate system scheme, that is an arithmetic average of the effective properties of the two types of interpenetrated planar arrays, also obtained from Eq. (14) with the appropriate layer orientation and fiber inter-distance. This second description is not either fully satisfying for the interactions between the two interpenetrated arrays are still not well accounted for. In this example, a better account for all the fiber interactions would be likely obtained in considering at once these two pairs of planar alignments in a four-layer laminate system scheme.

Now, since the structure of Fig. 9 right can also be described as two inter penetrated ($\pm\phi$) 1D rectangular fiber bundles, a property estimate can also be obtained from using a two-term fiber system scheme that consists in the (arithmetic) average of the effective properties for these two rectangular bundles, the effective properties of which can be obtained as for the hexagonal bundle discussed in the previous section, by construction of the global bundle operator from the (two orthogonal), appropriately rotated, operator of infinite planar alignments.

The best appropriate choice for a specific structure will be detail-dependant, and we do not enter further into this here. The goal of this last section is limited to introduce how, from the obtained global operators for infinite planar alignments and, from them, for 1D bundles of infinite fibers, possibly deformable and with element interactions essentially (if not fully) accounted for, relevant estimates are made available for fiber network-reinforced matrices. Further description of the evolution under strain of such networks depends on their "behavior law" which is still to be specified and in particular on the interconnections that may exist between the fibers of a same layer or of different ones. These interconnections between fibers are of determinant role in most networked structures. They can go, as exemplified in Fig. 1, from simple contacts to physical connections, as for the pantographic-like structures of Fig. 1 right, the homogeneous domains of which obeys a classic first gradient material [69–72]. When assumed embedded in a compliant matrix, the here introduced effective property estimates for such structures from the study of infinite alignments of interacting infinite fibers are relevant down to infinitesimal matrix stiffness, as will be addressed in a forthcoming paper dedicated to planar alignments of parallel beams with any rectangular cross section.

5 Conclusion

In order to estimate effective properties of compliant matrices reinforced with deformable fiber networks, we have first analytically derived global (interior plus interaction parts of) mean Green operators for large, and up to infinite, planar alignments of parallel cylindrical fibers of infinite length in isotropic matrices, the also solved case of rectangular beams being to be presented separately. The mean pair interaction operator between two infinite parallel cylinders is the first obtained and here presented original theoretical result, from which the mean interaction operator for infinite planar alignments of parallel identical cylinder (with equal inter-distances) appears of very simple closed form (thanks to the used Radon transform and inverse transform method). This interaction operator for infinite planar alignments of cylinders is an even polynomial form of order four in terms of the fiber radius to inter-distance ratio, similar to order five odd polynomial form of the interaction operator for infinite alignments of equally distant identical spheres, as reported in a previous

work. Owing to the infinite length of the fibers and to the co-continuity, they ensure with the matrix in the fiber directions, the operator for infinite planar alignments opens on specific interest for network-reinforced matrices.

It has been shown that the influence distance between two fibers, that is the fiber neighborhood within which interactions matter in a global pattern operator, is typically one order of magnitude (ten to twenty times) larger than the fiber cross section radius. This allows to making use of the infinite alignment operator for any planar fiber array larger than ten to twenty fibers if they are likely to all get close to each other, or even less according to the minimal inter-distance between them. The inter-distance between the fibers is the key parameter that modifies the number of fibers in this fixed influence zone. The 2D shape of this influence zone is assigned by the fiber cross section shape and by the symmetry properties of the matrix. It is in particular 2D isotropic around circular fibers in transversally isotropic matrices.

It has been then shown how these global mean operators for infinite planar alignments of fibers can provide global mean operators for one-directional fiber bundles in averaging a finite operator set for coaxial dense planar alignments to be quite easily used in homogenization frameworks for effective property estimates of directionally fiber-reinforced matrices. A first key interest is the possibility to quite easily follow the effective property variations related to deformation-like changes in such 1D fiber networks when embedded in a soft matrix with a much better accuracy in capturing the property variations than when using a too small finite pattern that is only valid for dilute concentrations of the chosen pattern. Furthermore, the use of an infinite pattern in accounting for the major (and possibly all if necessary) pair interactions between the inclusions interior to the influence zone by-passes the dilute and no interaction approximation suffered by the mean field estimates from the literature and extends their validity range to the maximal element (here fiber) concentrations allowed by the no-overlap limit.

It is finally shown how extension to determining, from the obtained effective properties for 1D bundles, the effective properties for a matrix reinforced with interpenetrated multi-directional fiber networks is possible, thanks to the building of global mean operator for the whole network and to the use of laminate system and fiber system schemes. The case of networks with interconnected fibers, as in particular typical pantographic-like beam structures of increasing interest, will be the topic of a dedicated forthcoming paper.

Acknowledgements Mario Spagnuolo has received funding from the European Union's Horizon 2020 research and innovation programme under the Marie Skłodowska-Curie Grant agreement No. 665850.

Appendix A: Recall of the bases of the RT/IRT method, from [36,42] and following works

In an infinite homogeneous elastic medium of $\mathbf{C}$ elasticity moduli, the $\mathbf{G}(\mathbf{r}-\mathbf{r}')$ Green "strain" tensor, gives the $\mathbf{u}(\mathbf{r})$ displacement field at point $\mathbf{r} = (x_1,\ x_2,\ x_3)$ due to a punctual force $\mathbf{F}(\mathbf{r}')$ at point $\mathbf{r}'$ by the relation $u_i(\mathbf{r}) = G_{ij}(\mathbf{r}-\mathbf{r}')\ F_j(\mathbf{r}')$. This tensor is classically defined by the equation $C_{mnpq}\ G_{pj,qn}(\mathbf{r}-\mathbf{r}') + \boldsymbol{\delta}(\mathbf{r}-\mathbf{r}')\ \Delta_{mj} = 0$, issued from explicating the stress equilibrium condition of linear elasticity $\boldsymbol{\sigma}_{ij,j}(\mathbf{r}) = C_{ijkl}\boldsymbol{\varepsilon}_{kl,j}(\mathbf{r}) = 0.5C_{ijkl}\left(u_{k,lj}(\mathbf{r}) + u_{l,kj}(\mathbf{r})\right) = 0$, where Δ is the Kronecker tensor and $\boldsymbol{\delta}(\mathbf{r})$ is the delta (generalized) function in R^3. Introducing the notations $\Gamma_{pqjn}(\mathbf{r}-\mathbf{r}') = -\ G_{pj,qn}(\mathbf{r}-\mathbf{r}')\big|_{((p,q),(j,n))}$, with '$((p,q),(j,n))$' specifying the symmetry on each pair of indices within brackets plus the super-symmetry of the two index pairs, the $\Gamma_{pqjn}(\mathbf{r}-\mathbf{r}')$ operator, is the twice differentiated Green operator generally called the modified Green operator. The integral of this Go over a bounded V domain (possibly an inclusion pattern) which depends on the V domain shape and on the $\mathbf{C}$ elasticity moduli of the matrix containing V, say $t^V_{pqjn}(\mathbf{r}) = \int_V \Gamma_{pqjn}(\mathbf{r}-\mathbf{r}')\ \mathrm{d}\mathbf{r}'$, can be calculated from the Fourier transform of the force versus displacement relation that reads $C_{mnpq}\ \breve{G}_{pj}(\mathbf{K})\ k_q\ k_n = \Delta_{mj}$, where $\mathbf{K} = (k_1,\ k_2,\ k_3)$ and $|\mathbf{K}| = k$. In spherical coordinates such that $k_i = k\ \omega_i$, $\mathbf{K} = k\ \boldsymbol{\omega}$, with $\boldsymbol{\omega} = (\sin\theta\cos\varphi, \sin\theta\sin\varphi, \cos\theta)$, this formula can be explicated as $C_{mnpq}\ \omega_q\ \omega_n\ k^2\ \breve{G}_{pj}(\mathbf{K}) = M_{mp}(\boldsymbol{\omega})\ k^2\ \breve{G}_{pj}(\mathbf{K}) = \Delta_{mj} \Rightarrow k^2\ \breve{G}_{pj}(\mathbf{K}) = (M^{-1})_{pj}(\boldsymbol{\omega})$ where the $k^2\ \breve{G}_{pj}(\mathbf{K})$ product is independent on the k modulus of the K vector. Next, replacing $\Gamma_{pqjn}(\mathbf{r}-\mathbf{r}')$ by the inverse transform of its Fourier transform yields:

$$t^V_{pqjn}(\mathbf{r}) = \frac{1}{8\ \pi^3}\ \int_V \left(\int \left((M^{-1})_{pj}(\boldsymbol{\omega})\ \omega_q\ \omega_n\right)\big|_{((pq),(jn))} \exp^{-i\ \mathbf{K}\ (\mathbf{r}-\mathbf{r}')} \mathrm{d}\mathbf{K} \right) \mathrm{d}\mathbf{r}', \tag{A.1}$$

from which, writing $\mathrm{d}\mathbf{K} = k^2 \mathrm{d}k \sin\theta \mathrm{d}\theta \mathrm{d}\varphi = k^2 \mathrm{d}k \mathrm{d}\omega$, one obtains the operator form:

$$t^V_{pqjn}(\mathbf{r}) = \frac{1}{8\,\pi^3} \int_V \left(\int_\Omega t^e_{pqjn}(\omega) \int_{k=0}^{\infty} k^2 \exp^{-i\,\mathbf{K}\,(\mathbf{r}-\mathbf{r}')}\,\mathrm{d}k\mathrm{d}\omega \right) \mathrm{d}\mathbf{r}', \tag{A.2}$$

where Ω is the unit sphere. Permutation of the V and Ω integrals ends to formally write:

$$t^V_{pqjn}(\mathbf{r}) = \int_\Omega t^e_{pqjn}(\omega)\ \psi_V(\omega, \mathbf{r})\ \mathrm{d}\omega, \tag{A.3}$$

with:

$$\psi_V(\omega, \mathbf{r}) = \frac{1}{8\,\pi^3} \int_V \left(\int_{k=0}^{\infty} k^2\ \exp^{-ik\boldsymbol{\omega}(\mathbf{r}-\mathbf{r}')\,\mathrm{d}k} \right) \mathrm{d}\mathbf{r}', \tag{A.4a}$$

$$t^e_{pqjn}(\omega) = \left((M^{-1})_{pj}(\omega) \omega_q\ \omega_n \right)_{((pq),(jn))}. \tag{A.4b}$$

Obviously, whatever the V domain shape is, $\mathbf{t}^V(\mathbf{r})$ writes under the form of a weighted angular average of $\mathbf{t}^e(\omega)$ elementary operators, with a $\psi_V(\omega, \mathbf{r})$ weight function. Then, taking a (x, y, z) frame with Oz // $\mathbf{K}$ // $\boldsymbol{\omega}$, such that $\mathbf{K} \times \mathbf{r} = k\boldsymbol{\omega} \times \mathbf{r} = k\ z$, Eq. (A.4a) reads:

$$\psi_V(\omega, \mathbf{r}) = \frac{1}{8\,\pi^3} \left(-\frac{1}{2} \int_V \left(\int_{-\infty}^{+\infty} (i\ t)^2\ \exp^{-i\ t\ (z-z')}\ \mathrm{d}t \right) \mathrm{d}\mathbf{r}' \right) = -\frac{1}{8\,\pi^2} \int_V \delta''(z - z', \omega)\ \mathrm{d}\mathbf{r}', \tag{A.5}$$

with $\delta''(z - z', \omega)$, the second z-derivative of the one-dimensional delta function, $\boldsymbol{\omega}$ both defining a direction in space and the infinite z-oriented axis along this direction. Setting $\mathrm{d}\mathbf{r}' = \mathrm{d}s_V(z', \omega)\ \mathrm{d}z'$, with $s_V(z', \omega)$ the area of the section of the volume V by the plane of $z' = \boldsymbol{\omega}.\mathbf{r}'$ equation, yields:

$$\psi_V(\omega, \mathbf{r}) = -\frac{1}{8\,\pi^2} \int_{z'=-\infty}^{z'=+\infty} \left(\int_{s_V(z',\omega)} \mathrm{d}s_V(z', \omega) \right) \delta''(z - z', \omega)\ \mathrm{d}z' = -\frac{1}{8\,\pi^2}\ s_{V''}(z, \omega), \tag{A.6}$$

where $s''_V(z, \omega)$ is the second z-derivative of $s_V(z, \omega)$. Since V is bounded, the z' integral in Eq. (A.6) is only nonzero within the $\left\lfloor D^-_V(\omega), D^+_V(\omega) \right\rfloor = 2\ D_V(\omega)$ breadth of V in the $\boldsymbol{\omega}$ direction, i-e the distance between the two opposite tangent planes to V, of $\boldsymbol{\omega}$-normal. These definitions likely hold as well for single domains or for sets of regular subdomains, in which cases the $2\ D_V(\omega)$ breadths characterize the support function of the convex hull of V and the z' integral over $\left\lfloor D^-_V(\omega), D^+_V(\omega) \right\rfloor$ dissociates into several ones over separated intervals. $\psi_V(\omega, \mathbf{r})$ is not uniform in V except when it is an isolated ellipsoidal volume. The $\overline{\psi_V}(\omega)$ mean value of $\psi_V(\omega, \mathbf{r})$ over V, which appears in the $\overline{\mathbf{t}^V} = \frac{1}{v} \int_V \mathbf{t}^V(\mathbf{r}) \mathrm{d}\mathbf{r}$ volume average of $\mathbf{t}^V(\mathbf{r})$, is obtained setting $\mathrm{d}\mathbf{r} = \mathrm{d}s_V(z, \omega)\ \mathrm{d}z$, as for $\mathrm{d}\mathbf{r}$' in $\psi_V(\omega, \mathbf{r})$, and with the area integral part directly written $s_V(z, \omega)$, what arrives at:

$$\overline{\psi_V}(\omega) = -\frac{1}{8\pi^2 v} \int_{D^-_V(\omega)}^{D^+_V(\omega)} \tilde{s}_{V''}(z, \omega)\ s_V(z, \omega)\ \mathrm{d}z = \frac{1}{8\pi^2 v} \int_{D^-_V(\omega)}^{D^+_V(\omega)} (\tilde{s}_{V'}(z, \omega))^2\ \mathrm{d}z, \tag{A.7}$$

The right hand side of Eq. (A.7) results from part integration, and the tilde on the z-derivatives of $s_V(z, \omega)$ indicates that their regularized form needs to be considered. See cited references for further details.

Appendix B: The mean Green interaction operator between two infinite parallel cylinders

Main calculation steps are in part $B1$, additional calculation details are given in parts $B2$ and $B3$. Let first recall that for an ellipsoid $V0$, what includes the infinite cylinders with elliptic or circular cross section at limit (together with zero-thickness platelets at the other extreme), the interior uniform weight function takes the simple form (wit $z = \boldsymbol{\omega}.\mathbf{r}$ and $\left\lfloor -D^{\mathrm{ell}}_V(\boldsymbol{\omega}), D^{\mathrm{ell}}_V(\boldsymbol{\omega}) \right\rfloor$ the breadth of $V0$ in the $\boldsymbol{\omega}$-normal direction):

$$\psi^{\mathrm{ell}}_{V0}(\boldsymbol{\omega}) = \left(-\frac{1}{8\pi^2} \right) \frac{\partial^2}{\partial z^2} \left(\frac{3\ v}{4\ D^{\mathrm{ell}}_{V0}(\boldsymbol{\omega})} \left(1 - \left(\frac{z}{D^{\mathrm{ell}}_{V0}(\boldsymbol{\omega})} \right)^2 \right) \right) \quad = \quad \left(\frac{3}{4\ \pi} \right)^2 \left(\frac{v}{3\ D^{\mathrm{ell}}_{V0}(\boldsymbol{\omega})^3} \right).$$

-**B1**: For two ellipsoids $V1$, $V2$ (of volume $v1$ and $v2$, respectively), with centers I1,I2 at distance $\pm L$ from the frame origin O along the $x3$ axis, the weight function to be calculated reads [42]:

$$\overline{\psi_v^{V1,V2}}(\omega) = \int_{z_{(\omega)}^{\min}}^{z_{(\omega)}^{\max}} \frac{2\left(s'_{V1}(z+\eta_\omega,\omega)s_{V2'}(z-\eta_\omega,\omega)\right)}{8\pi^2 v}\mathrm{d}z = \frac{P_{(1,2)}}{D_1(\omega)^3 D_2(\omega)^3}\left(\frac{z^3}{3}-\eta_\omega^2 z\right)_{z_{(\omega)}^{\min}}^{z_{(\omega)}^{\max}}, \quad \text{(B.1)}$$

with $P_{(1,2)} = \frac{9v1v2}{16\pi^2(v1+v2)}$. $s'_{Vi}(z,\omega)$ is the first z-derivative of the section area of Vi by the plane of equation $z = \boldsymbol{\omega}.\mathbf{r}$, $D_1(\omega)$ is the breadth of Vi in direction $\boldsymbol{\omega} = (\theta,\phi)$ and $\eta_\omega = L\cos\theta$. The direction $\omega = (0,\phi)$ corresponds $\forall\phi$ to the $x3$ axis around which θ is counted and ϕ runs in the $x1$–$x2$ plane from 0 along direction $x1$. Taking η_ω positive corresponding to the half $\theta \in (0,\pi/2)$ domain, Eq. (B.1) yields, with $\left\{z^{\min}, z^{\max}\right\} = \{\eta - D_2, D_1 - \eta\}$ for $0 \le \eta \le (D_1+D_2)/2$ (the ω-dependencies are here omitted for brevity) and with $D_1 = D_2 = D0(\omega)\forall\omega$ when $V1 = V2 = V0$:

$$\overline{\psi_v^{V1,V2}}(\omega) = \frac{P_{(1,2)}}{D_1^3 D_2^3}\left(\frac{D_1^3}{3}+\frac{D_2^3}{3}-\eta\left(D_1^2+D_2^2\right)+\frac{4\eta^3}{3}\right), \forall\phi. \quad \text{(B.2)}$$

For spheroids of semi-axes (a,c,a) with $c//x_2$, $c/a = \zeta => 1$ and volume $v_0 = 4\pi a^3\zeta/3$ such that $P_{(1,2)} = P = \frac{9v_0^2}{16\pi^2(2v_0)} = \frac{3a^3\zeta}{8\pi}$, the breadths read $D_0(\theta,\phi) = a\sqrt{1+\left(\zeta^2-1\right)\sin^2\phi\sin^2\theta} = a\sqrt{1+\left(\lambda^2(\phi)-1\right)\sin^2\theta}$ and the interior and interaction weight functions:

$$\psi_{x2}^{\zeta-\mathrm{sph}}(\theta,\phi) = \frac{1}{4\pi}\frac{\zeta}{\left(1+\left(\boldsymbol{\zeta}^2-1\right)\sin^2\phi\sin^2\theta\right)^{3/2}} = \frac{1}{4\pi}\frac{\zeta}{\left(1+\left(\lambda(\phi)^2-1\right)\sin^2\theta\right)^{3/2}},$$

$$\overline{\psi_{x2(x1)}^{2\mathrm{sph}\zeta}}(\theta,\phi) = \frac{P}{D_0^6(\theta,\phi)}\left(\frac{2D_0^3(\theta,\phi)}{3}-2\boldsymbol{\eta}_{(\theta,\phi)}D_0(\theta,\phi)^2+\frac{4\eta_{(\theta,\phi)}^3}{3}\right) \quad \text{(B.3a)}$$

$$= \frac{\zeta}{4\pi}\left(\frac{1}{\left(1+(\lambda(\phi)^2-1)\sin^2\theta\right)^{3/2}}-\frac{3(L/a)\cos\theta}{\left(1+(\lambda(\phi)^2-1)\sin^2\theta\right)^2}+\frac{2(L/a)^3\cos^3\theta}{\left(1+(\lambda(\phi)^2-1)\sin^2\theta\right)^3}\right). \quad \text{(B.3b)}$$

Equation B.3 can be formally written:

$$\overline{\psi_{x2(x1)}^{2\mathrm{sph}\zeta}}(\theta,\phi) = I_{2\mathrm{sph}\zeta}^{0,0} = \sum_{i(m,n)=1}^{3} F_{i(m,n)}^{0,0}(\theta,\phi) = \sum_{i(m,n)=1}^{3}\frac{\zeta}{4\pi}K_{i(m,n)}\frac{\cos^m\theta}{\left(1+(\lambda(\phi)^2-1)\sin^2\theta\right)^n}, \quad \text{(B.4)}$$

the three elements $i(m,n) = 1,2,3$ of which correspond to $(m,n) = (0,3/2),(1,2),(3,3)$ and with the appropriate coefficients, $K_{i(m,n)} = 1, -3L/a = -3/\rho_0$ and $2(L/a)^3 = 2/\rho_0^3$ as appearing. For an isotropic reference matrix, the integrals to be calculated belong to the set:

$$I_{2\mathrm{sph}\zeta}^{p,q} = \sum_{i(m,n)=1}^{3} I_{i(m,n)}^{p,q} = \sum_{i(m,n)=1}^{3}\left(\int_{\phi=0}^{2\pi} 2\int_{\theta=\theta_{\min}}^{\pi/2} F_{i(m,n)}^{p,q}(\theta,\phi)\sin\theta\mathrm{d}\theta\mathrm{d}\phi\right), \quad p,q = 0,1,2, \quad \text{(B.5)}$$

$$\text{where:} \quad F_{i(m,n)}^{p,q}(\theta,\phi) = \frac{\zeta}{4\pi}K_{i(m,n)}\frac{\cos^m\theta}{\left(1+(\lambda(\phi)^2-1)\sin^2\theta\right)^n}\cos^{2p}\theta\cos^{2q}\phi. \quad \text{(B.6)}$$

The value of $\theta_{\min}$which depends on ϕ corresponds with $\tan(\theta_{\min}) = \tan(\theta(\phi)_{\min}) = \frac{1}{\lambda(\phi)}\sqrt{\frac{L^2-a^2}{a^2}}$. $\theta_{\min} = 0$ when $L = a$ (contact) for all ϕ angles. Then, with $1+\tan^2(\theta_{\min}) = \cos^{-2}(\theta_{\min})$, it comes:

$$\cos(\theta(\phi)_{\min}) = \sqrt{\frac{\lambda^2(\phi)}{\left(\lambda^2(\phi)-1\right)+\left(L^2/a^2\right)}} = \frac{\rho_0\lambda(\phi)}{\sqrt{\rho_0^2\lambda^2(\phi)+\left(1-\rho_0^2\right)}} = \rho(\phi) \le \rho_0 \le 1. \quad \text{(B.7)}$$

The case $p, q = 0, 0$ in Eqs. (B.5), (B.6) corresponds to the integrals of the elements of the mean pair interaction weight function itself in Eq. (B.1), for which we know that they always fulfill together the null value $\int_{\phi=0}^{2\pi} 2 \int_{\theta=\theta_{\min}}^{\pi/2} \overline{\psi_v^{V1,V2}}(\theta, \phi) \sin\theta \mathrm{d}\theta\mathrm{d}\phi = \sum_{i(m,n)=1}^{3} \left(\int_{\phi=0}^{2\pi} 2 \int_{\theta=\theta_{\min}}^{\pi/2} F_{i(m,n)}^{0,0}(\theta, \phi) \sin\theta \mathrm{d}\theta\mathrm{d}\phi \right) = 0$. As will appear next on, for parallel infinite cylinders, only the cases $p = 0, 1, 2$ with $q = 0$ suffice to obtain all the interaction operator terms, say nine double integrals of the generic form:

$$I_{i(m,n)}^{p,0} = \int_{\phi=0}^{2\pi} 2 \int_{\theta=\theta_{\min}}^{\pi/2} F_{i(m,n)}^{p,0}(\theta, \phi) \sin\theta \mathrm{d}\theta\mathrm{d}\phi = 8 \int_{\phi=0}^{\pi/2} \int_{\theta=\theta_{\min}}^{\pi/2} F_{i(m,n)}^{p,0}(\theta, \phi) \sin\theta \mathrm{d}\theta\mathrm{d}\phi$$
$$= \frac{8\zeta}{4\pi} K_{i(m,n)} \int_{\phi=0}^{\pi/2} \int_{\theta=\boldsymbol{\theta}_{\min}}^{\pi/2} \left(\frac{\cos^m\theta}{\left(1 + (\lambda(\phi)^2 - 1)\sin^2\theta\right)^n} \cos^{2p}\theta \right) \sin\theta \mathrm{d}\theta\mathrm{d}\phi. \tag{B.8}$$

The variable changes $\cos\theta = x$ and $\lambda(\phi)^2 - 1 = \alpha(\phi)^{-2} \geq 0$ (for prolate spheroids[11]) yield:

$$I_{i(m,n)}^{p,0} = \frac{2\zeta}{\pi} K_{i(m,n)} \int_{\phi=0}^{\pi/2} \left(\alpha(\phi)^{2n} \int_{x=0}^{x_{mx}} \frac{x^{m+2p}\mathrm{d}x}{\left(1 + \alpha(\phi)^2 - x^2\right)^n} \right) \mathrm{d}\phi = \frac{2\zeta}{\pi} K_{i(m,n)} \int_{\phi=0}^{\pi/2} G_{m,n}^{p,0}(\alpha(\phi)) \mathrm{d}\phi, \tag{B.9}$$

where $x_{mx} = x_{\max}(\phi) = \cos(\theta(\phi)_{\min}) = \rho(\phi)$. The calculation steps for the nine x-integrals $G_{m,n}^{p,0}(\alpha(\phi))$ are given in **part B2**. Also using $x_{mx}^2 = \frac{\rho_0^2(1+\alpha^2)}{\rho_0^2+\alpha^2}$ and $\frac{x_{mx}^2}{1+\alpha^2-x_{mx}^2} = \frac{\rho_0^2}{\alpha^2}$ where α stands for $\alpha(\phi)$, one arrives at the 9 forms:

$$G_{0,3/2}^{0,0}(\alpha) = \frac{\alpha^2}{1+\alpha^2}\rho_0, \tag{B.10a}$$
$$G_{0,3/2}^{1,0}(\alpha) = \alpha^3 \left(\frac{\rho_0}{\alpha} - \tan^{-1}\left(\frac{\rho_0}{\alpha}\right) \right), \tag{B.10b}$$
$$G_{0,3/2}^{2,0}(\alpha) = \frac{\left(\alpha^3 + \alpha^5\right)}{2} \left(\frac{\rho_0\alpha}{\rho_0^2 + \alpha^2} + 2\frac{\rho_0}{\alpha} - 3\tan^{-1}\left(\frac{\rho_0}{\alpha}\right) \right), \tag{B.10c}$$

$$G_{1,2}^{0,0}(\alpha) = \frac{\alpha^2}{1+\alpha^2}\frac{\rho_0^2}{2}, \tag{B.11a}$$
$$G_{3,3}^{0,0}(\alpha) = \frac{\alpha^2}{1+\alpha^2}\frac{\rho_0^4}{4}, \tag{B.11b}$$

$$G_{1,2}^{1,0}(\alpha) = \frac{\alpha^4}{2} \left(\frac{\rho_0^2}{\alpha^2} - \ln\left(\frac{\rho_0^2 + \alpha^2}{\alpha^2}\right) \right), \tag{B.12a}$$
$$G_{3,3}^{1,0}(\alpha) = \frac{\alpha^6}{2} \left(\frac{1}{2}\frac{\rho_0^4}{\alpha^4} - \frac{\rho_0^2}{\alpha^2} + \ln\left(\frac{\alpha^2 + \rho_0^2}{\alpha^2}\right) \right), \tag{B.12b}$$

$$G_{1,2}^{2,0}(\alpha) = \frac{\left(\alpha^4 + \alpha^6\right)}{2} \left(\frac{\rho_0^2}{\alpha^2} + \frac{\rho_0^2}{\rho_0^2 + \alpha^2} - 2\ln\left(\frac{\alpha^2 + \rho_0^2}{\alpha^2}\right) \right), \tag{B.13a}$$
$$G_{3,3}^{2,0}(\alpha) = \frac{\left(\alpha^6 + \alpha^8\right)}{2} \left(\frac{1}{2}\frac{\rho_0^4}{\alpha^4} + 3\ln\left(\frac{\rho_0^2 + \alpha^2}{\alpha^2}\right) - \frac{\rho_0^2}{\rho_0^2 + \alpha^2} - 2\frac{\rho_0^2}{\alpha^2} \right). \tag{B.13b}$$

Equations (B.10)–(B.13) also hold for more general ellipsoids than $x2$-oriented spheroids ($\beta = 1$), using $\lambda(\phi)^2 - 1 = \alpha(\phi)^{-2} = \left(\zeta^2 - \beta^2\right)\sin^2\phi + \left(\beta^2 - 1\right) \geq 0$ in Eq. (B.3) and following ones. At the sphere

[11] The case of oblate spheroids (to be treated) follows the same route, using $1 - \lambda(\phi)^2 = \alpha(\phi)^{-2} \geq 0$.

pair limit ($\beta = 1, \zeta = 1$), the ϕ integrals becomes independent of θ and simply amounts to multiplying the functions $G^{p,0}_{m,n}(\alpha)$ by a factor $\pi/2$ in Eq. (B.9) with the value for α being its infinite limit. Taking the $\alpha \to \infty$ (or $\bar{\alpha} \to 0$) limits in Eqs. (B.10)–(B.13) well provides the sphere pair expected values, as recalled in part B2 (elliptic cross sections $\beta \neq 1$ yield a $(\beta, 1, 1)$ spheroid pair limit).
Back to the $x2$-oriented spheroids, the second ϕ integrations in Eq. (B.9) with using the obtained functions $G^{p,0}_{m,n}(\alpha(\phi))$ are solved using a second (ϕ to α) variable change from $\alpha(\phi)^2 = \frac{1}{\lambda(\phi)^2-1} = \frac{\sin^{-2}(\phi)}{\zeta^2-1}$, what yields $\frac{d(\alpha(\phi)^2)}{\mathrm{d}\phi} = -2\frac{\sin^{-3}(\phi)}{\zeta^2-1}\cos(\phi) = -\frac{2\alpha(\phi)^2}{\tan(\phi)}$ such that $\mathrm{d}\phi = -\tan(\phi)\frac{\mathrm{d}\alpha}{\alpha}$ with $\tan(\phi) = \left((\zeta^2-1)\alpha^2-1\right)^{-1/2}$. That finally arrives at $\mathrm{d}\phi = -\left((\zeta^2-1)\alpha^2-1\right)^{-1/2}(\mathrm{d}\alpha/\alpha)$. The reference integral form becomes:

$$I^{p,0}_{i(m,n)} = \frac{2\zeta}{\pi} K_{i(m,n)} \int_{\phi=0}^{\pi/2} G^{p,0}_{m,n}(\alpha(\phi))\mathrm{d}\phi = \frac{2\zeta}{\pi} K_{i(m,n)} \int_{\alpha=(\zeta^{\infty 2}-1)^{-1/2}}^{\infty} \frac{G^{p,0}_{m,n}(\alpha)}{\sqrt{(\zeta^2-1)\alpha^2-1}} \frac{\mathrm{d}\alpha}{\alpha}. \tag{B.14a}$$

This complicated integral type simplifies for infinite cylindrical fibers $\zeta \to \infty$ as:

$${}^{\zeta^\infty}I^{p,0}_{i(m,n)} = \frac{2}{\pi}\frac{K_{i(m,n)}\zeta^\infty}{\sqrt{\zeta^{\infty 2}-1}} \int_{\alpha=(\zeta^{\infty 2}-1)^{-1/2}}^{\infty} \frac{G^{p,0}_{m,n}(\alpha)}{\sqrt{\alpha^2-(\zeta^{\infty 2}-1)^{-1}}} \frac{\mathrm{d}\alpha}{\alpha} \to \frac{2}{\pi} K_{i(m,n)} \int_{\alpha=0}^{\infty} \frac{G^{p,0}_{m,n}(\alpha)}{\alpha} \frac{\mathrm{d}\alpha}{\alpha}. \tag{B.14b}$$

Analytical solutions are obtained as shown in **part B3** for the 9 integrals, either from the direct α integration or in terms of its inverse $\bar{\alpha} = 1/\alpha$, since $\int_{\alpha=0}^{\infty} G^{p,0}_{m,n}(\alpha)\left(\mathrm{d}\alpha/\alpha^2\right) = \int_{\bar{\alpha}=0}^{\infty} G^{p,0}_{m,n}(\bar{\alpha})\mathrm{d}\bar{\alpha}$ (infinite elliptic fibers, $\beta \neq 1$ and $\zeta \to \infty$, here disregarded can be treated similarly).
The variable change from ϕ to α highlights why integrals of Eq. (B.9) with $q = 1, 2$ as $I^{p,q}_{i(m,n)} = (2\zeta/\pi)\, K_{i(m,n)} \int_{\phi=0}^{\pi/2} G^{p,q}_{m,n}(\alpha(\phi))\cos^{2q}(\phi)\mathrm{d}\phi$ are equal to the corresponding $I^{p,0}_{i(m,n)}$ integral when $\zeta \to \infty$: with using $\cos^{2q}(\phi) = \left(1 - \frac{1}{(\zeta^2-1)\alpha^2}\right)^q$, Eq. (B.14a) becomes:

$${}^{\zeta^\infty}I^{p,q}_{i(m,n)} = \frac{2}{\pi}\frac{K_{i(m,n)}\zeta^\infty}{\sqrt{\zeta^{\infty 2}-1}} \int_{\alpha=(\zeta^{\infty 2}-1)^{-1/2}}^{\infty} \frac{G^{p,0}_{m,n}(\alpha)}{\sqrt{\alpha^2-(\zeta^{\infty 2}-1)^{-1}}} \left(1 - \frac{1}{(\zeta^{\infty 2}-1)\alpha^2}\right)^q \frac{\mathrm{d}\alpha}{\alpha}. \tag{B.15}$$

When $\zeta \to \infty$, this additional factor equals unity for any nonzero α value and does not affect the integral such that $\lim_{\zeta\to\infty} I^{p,q}_{i(m,n)} = \lim_{\zeta\to\infty} I^{p,0}_{i(m,n)}$, $q = 1, 2$. For the same reason, as is easily verified for the integrals that correspond to the terms of the cylinder interior weight function and interior operator, which are known from direct simple calculation, one has $\lim_{\zeta\to\infty}(2\zeta/\pi)\, K_{i(m,n)} \int_{\phi=0}^{\pi/2} G^{p,q}_{m,n}(\alpha(\phi))\sin^{2q}(\phi)\mathrm{d}\phi = 0$.
-B2: Integrals with regard to $x = \cos\theta$. For $n = 3/2$, one obtains, taking $u = \frac{x}{\sqrt{1+\alpha^2}}$:

$$1^\circ)\quad G^{0,0}_{0,3/2}(\alpha) = \alpha^3 \int_0^{x_{mx}} \frac{\mathrm{d}x}{\left(1+\alpha^2-x^2\right)^{3/2}} = \frac{\alpha^3}{1+\alpha^2} \int_0^{u_{mx}} \frac{\mathrm{d}u}{\left(\sqrt{1-u^2}\right)^3} = \frac{\alpha^3}{1+\alpha^2}\frac{u_{mx}}{\sqrt{1-u^2_{mx}}}$$
$$= \frac{\alpha^3}{1+\alpha^2}\sqrt{\frac{x^2_{mx}}{1+\alpha^2-x^2_{mx}}} = \frac{\alpha^3}{1+\alpha^2}\frac{\rho_0}{\alpha} = \rho_0\frac{\alpha^2}{1+\alpha^2}\left(\lim\nolimits^{\text{sphere}}_{\alpha\to\infty} = \rho_0\right);$$

$$2^\circ)\quad G^{1,0}_{0,3/2}(\alpha) = \alpha^3 \int_0^{x_{mx}} \frac{x^2\mathrm{d}x}{\left(1+\alpha^2-x^2\right)^{3/2}} = \alpha^3 \int_0^{u_{mx}} \frac{1-\left(1-u^2\right)}{\left(1-u^2\right)^{3/2}}\mathrm{d}u$$
$$= \alpha^3\left(\sqrt{\frac{x^2_{mx}}{1+\alpha^2-x^2_{mx}}} - \sin^{-1}\left(\sqrt{\frac{x^2_{mx}}{1+\alpha^2}}\right)\right) = \alpha^3\left(\frac{\rho_0}{\alpha} - \tan^{-1}\left(\frac{\rho_0}{\alpha}\right)\right)\left(\lim\limits^{\text{sphere}}_{\bar{\alpha}\to 0} = \frac{\rho_0^3}{3}\right);$$

In Eq. B2.2°, we have used $\sin^{-1}\left(\sqrt{\frac{\rho_0^2}{\rho_0^2+\alpha^2}}\right)=\tan^{-1}\left(\frac{\rho_0}{\alpha}\right)$.

$$3°)\quad G_{0,3/2}^{2,0}(\alpha)=\alpha^3\int_0^{x_{mx}}\frac{x^4\mathrm{d}x}{\left(1+\alpha^2-x^2\right)^{3/2}}=\alpha^3\left(1+\alpha^2\right)\left(\int_0^{u_{mx}}\frac{\left(1-u^2\right)^2+2u^2-1}{\left(1-u^2\right)^{3/2}}\mathrm{d}u\right)$$
$$=\alpha^3\left(1+\alpha^2\right)\frac{1}{2}\left(\sqrt{\frac{x_{mx}^2}{1+\alpha^2}}\sqrt{1-\frac{x_{mx}^2}{1+\alpha^2}}+2\sqrt{\frac{x_{mx}^2}{1+\alpha^2-x_{mx}^2}}-3\sin^{-1}\left(\sqrt{\frac{x_{mx}^2}{1+\alpha^2}}\right)\right)$$
$$=\left(\alpha^3+\alpha^5\right)\frac{1}{2}\left(\frac{\rho_0\alpha}{\rho_0^2+\alpha^2}+2\frac{\rho_0}{\alpha}-3\tan^{-1}\left(\frac{\rho_0}{\alpha}\right)\right)\left(\lim_{\tilde{\alpha}\to 0}^{\text{sphere}}=0\rho_0^3+\frac{\rho_0^5}{5}\right);$$

For the 6 remaining integrals (with $n=2$ and $n=3$), taking the variable change $z=\frac{x^2}{1+\alpha^2}$ yields:

$$4°)\quad G_{1,2}^{0,0}(\alpha)=\alpha^4\int_0^{x_{mx}}\frac{x\mathrm{d}x}{\left(1+\alpha^2-x^2\right)^2}=\frac{\alpha^4}{2\left(1+\alpha^2\right)}\int_0^{z_{mx}}\frac{\mathrm{d}z}{(1-z)^2}$$
$$=\frac{\alpha^4}{2\left(1+\alpha^2\right)}\left(\frac{x_{mx}^2}{1+\alpha^2-x_{mx}^2}\right)=\frac{\alpha^4}{2\left(1+\alpha^2\right)}\frac{\rho_0^2}{\alpha^2}=\frac{\alpha^2}{2\left(1+\alpha^2\right)}\rho_0^2\left(\lim_{\alpha\to\infty}^{\text{sphere}}=\frac{\rho_0^2}{2}\right);$$
$$5°)\quad G_{3,3}^{0,0}(\alpha)=\alpha^6\int_0^{x_{mx}}\frac{x^3\mathrm{d}x}{\left(1+\alpha^2-x^2\right)^3}=\frac{\alpha^6}{2\left(1+\alpha^2\right)}\left(\int_0^{z_{mx}}\frac{\mathrm{d}z}{(1-z)^3}-\int_0^{z_{mx}}\frac{\mathrm{d}z}{(1-z)^2}\right)$$
$$=\frac{1}{2}\left(\frac{x_{mx}^2}{1+\alpha^2-x_{mx}^2}\right)^2=\frac{\alpha^6}{2\left(1+\alpha^2\right)}\frac{1}{2}\left(\frac{\rho_0^2}{\alpha^2}\right)^2=\frac{\alpha^2}{4\left(1+\alpha^2\right)}\rho_0^4\left(\lim_{\alpha\to\infty}^{\text{sphere}}=\frac{\rho_0^4}{4}\right);$$
$$6°)\quad G_{1,2}^{1,0}(\alpha)=\alpha^4\int_0^{x_{mx}}\frac{x^3\mathrm{d}x}{\left(1+\alpha^2-x^2\right)^2}=\frac{\alpha^4}{2}\int_0^{z_{mx}}\frac{z\mathrm{d}z}{(1-z)^2}$$
$$=\frac{\alpha^4}{2}\left(\frac{x_{mx}^2}{(1+\alpha^2)-x_{mx}^2}+\ln\left(\frac{(1+\alpha^2)-x_{mx}^2}{1+\alpha^2}\right)\right)$$
$$=\frac{\alpha^4}{2}\left(\frac{\rho_0^2}{\alpha^2}-\ln\left(\frac{\rho_0^2+\alpha^2}{\alpha^2}\right)\right)\left(\lim_{\tilde{\alpha}\to 0}^{\text{sphere}}=\frac{\rho_0^4}{2}\right);$$
$$7°)\quad G_{3,3}^{1,0}(\alpha)=\alpha^6\int_0^{x_{mx}}\frac{x^5\mathrm{d}x}{\left(1+\alpha^2-x^2\right)^3}=\frac{\alpha^6}{2}\left(\frac{x_{mx}^2\left(3x_{mx}-2(1+\alpha^2)\right)}{2\left(1+\alpha^2-x_{mx}^2\right)^2}-\ln\left(\frac{1+\alpha^2-x_{mx}^2}{1+\alpha^2}\right)\right)$$
$$=\frac{\alpha^6}{2}\left(\left(\frac{1}{2}\frac{\rho_0^4}{\alpha^4}\right)-\left(\ln\left(\frac{\alpha^2}{\alpha^2+\rho_0^2}\right)+\frac{\rho_0^2}{\alpha^2}\right)\right)\left(\lim_{\tilde{\alpha}\to 0}^{\text{sphere}}=\frac{\rho_0^6}{6}\right);$$
$$8°)\quad G_{1,2}^{2,0}(\alpha)=\alpha^4\int_0^{x_{mx}}\frac{x^5\mathrm{d}x}{\left(1+\alpha^2-x^2\right)^2}=\frac{\alpha^4\left(1+\alpha^2\right)}{2}\int_0^{z_{mx}}\frac{z^2\mathrm{d}z}{(1-z)^2}$$
$$=\frac{\alpha^4\left(1+\alpha^2\right)}{2}\left(\frac{x_{mx}^2}{(1+\alpha^2)-x_{mx}^2}+2\ln\left(\frac{(1+\alpha^2)-x_{mx}^2}{1+\alpha^2}\right)+\frac{x_{mx}^2}{1+\alpha^2}\right)$$
$$=\frac{\left(\alpha^4+\alpha^6\right)}{2}\left(\frac{\rho_0^2}{\alpha^2}+\frac{\rho_0^2}{\rho_0^2+\alpha^2}-2\ln\left(\frac{\alpha^2+\rho_0^2}{\alpha^2}\right)\right)\left(\lim_{\tilde{\alpha}\to 0}^{\text{sphere}}=0\rho_0^4+\frac{\rho_0^6}{3}\right);$$

$$9^\circ)\quad G^{2,0}_{3,3}(\alpha)=\alpha^6\int\limits_0^{x_{mx}}\frac{x^7\mathrm{d}x}{\left(1+\alpha^2-x^2\right)^3}=\frac{\alpha^6\left(1+\alpha^2\right)}{2}\int\limits_0^{z_{mx}}\frac{z^3\mathrm{d}z}{(1-z)^3}$$
$$=\frac{\alpha^6\left(1+\alpha^2\right)}{2}\left(\frac{x_{mx}^2\left(5x_{mx}^2-4(1+\alpha^2)\right)}{2\left((1+\alpha^2)-x_{mx}^2\right)^2}-3\ln\left((1+\alpha^2)-x_{mx}^2\right)-(1+\alpha^2)x_{mx}^2\right)$$
$$=\frac{\left(\alpha^6+\alpha^8\right)}{2}\left(\frac{1}{2}\frac{\rho_0^4}{\alpha^4}+3\ln\left(\frac{\rho_0^2+\alpha^2}{\alpha^2}\right)-\frac{\rho_0^2}{\rho_0^2+\alpha^2}-2\frac{\rho_0^2}{\alpha^2}\right)\left(\lim\nolimits_{\alpha\to0}^{\text{sphere}}=0\rho_0^6+\frac{\rho_0^8}{8}\right);$$

-B3: Integrals with regard to $\alpha=\alpha(\phi)=\left((\zeta^2-1)\sin^2\phi\right)^{-1/2}$or $\kappa=\alpha/\rho_0$, at the limit $\zeta\to\infty$.

$$1^\circ)\quad {}^{\zeta^\infty}I^{0,0}_{0,3/2}=\frac{2}{\pi}K_{1(0,3/2)}\int\limits_{\alpha=0}^{\infty}\frac{G^{0,0}_{0,3/2}(\alpha)}{\alpha}\frac{\mathrm{d}\alpha}{\alpha}=\frac{2}{\pi}\int\limits_{\alpha=0}^{\infty}\frac{\alpha^2\rho_0}{1+\alpha^2}\frac{\mathrm{d}\alpha}{\alpha^2}=\rho_0,\ \lim\nolimits_{\rho_0\to1}^{\text{contact}}=1;$$

$$2^\circ)\quad {}^{\zeta^\infty}I^{1,0}_{0,3/2}=\frac{2}{\pi}K_{1(0,3/2)}\int\limits_{\alpha=0}^{\infty}\frac{G^{1,0}_{0,3/2}(\alpha)}{\alpha}\frac{\mathrm{d}\alpha}{\alpha}=\frac{2}{\pi}\int\limits_{\alpha=0}^{\infty}\alpha^3\left(\frac{\rho_0}{\alpha}-\tan^{-1}\left(\frac{\rho_0}{\alpha}\right)\right)\frac{\rho_0}{\alpha^2}d\left(\frac{\alpha}{\rho_0}\right)$$
$$=\frac{2\rho_0^2}{\pi}\int\limits_0^{\infty}\left(1-\kappa\tan^{-1}\left(\frac{1}{\kappa}\right)\right)\mathrm{d}\kappa=\frac{\rho_0^2}{2},\ \lim\nolimits_{\rho_0\to1}^{\text{contact}}=\frac{1}{2};$$

$$3^\circ)\quad {}^{\zeta^\infty}I^{2,0}_{0,3/2}=\frac{2}{\pi}K_{1(0,3/2)}\int\limits_{\alpha=0}^{\infty}\frac{G^{2,0}_{0,3/2}(\alpha)}{\alpha}\frac{\mathrm{d}\alpha}{\alpha}$$
$$=\frac{2}{\pi}\left(\frac{\rho_0^2}{2}\int\limits_{\kappa=0}^{\infty}\left(\frac{\kappa^2}{1+\kappa^2}+2-3\kappa\tan^{-1}\left(\frac{1}{\kappa}\right)\right)\mathrm{d}\kappa\right.$$
$$\left.+\frac{\rho_0^4}{2}\int\limits_{\kappa=0}^{\infty}\left(\frac{\kappa^4}{1+\kappa^2}+2\kappa^2-3\kappa^3\tan^{-1}\left(\frac{1}{\kappa}\right)\right)\mathrm{d}\kappa\right)$$
$$=\frac{2}{\pi}\left(\rho_0^2\frac{\pi}{8}+\rho_0^4\frac{\pi}{16}\right)=\frac{2\rho_0^2+\rho_0^4}{8},\ \lim\nolimits_{\rho_0\to1}^{\text{contact}}=\frac{3}{8};$$

$$4^\circ)\quad {}^{\zeta^\infty}I^{0,0}_{1,2}=\frac{2}{\pi}K_{2(1,2)}\int\limits_{\alpha=0}^{\infty}\frac{G^{0,0}_{1,2}(\alpha)}{\alpha}\frac{\mathrm{d}\alpha}{\alpha}=\frac{2}{\pi}\left(\frac{-3}{\rho_0}\right)\int\limits_{\alpha=0}^{\infty}\left(\frac{\alpha^2}{1+\alpha^2}\frac{\rho_0^2}{2}\right)\frac{\mathrm{d}\alpha}{\alpha^2}=-\frac{3\rho_0}{2},\ \lim\nolimits_{\rho_0\to1}^{\text{contact}}=\frac{-3}{2};$$

$$5^\circ)\quad {}^{\zeta^\infty}I^{0,0}_{3,3}=\frac{2}{\pi}K_{3(3,3)}\int\limits_{\alpha=0}^{\infty}\frac{G^{0,0}_{3,3}(\alpha)}{\alpha}\frac{\mathrm{d}\alpha}{\alpha}=\frac{2}{\pi}\left(\frac{2}{\rho_0^3}\right)\int\limits_{\alpha=0}^{\infty}\left(\frac{\alpha^2}{1+\alpha^2}\frac{\rho_0^4}{4}\right)\frac{\mathrm{d}\alpha}{\alpha^2}=\frac{\rho_0}{2},\ \lim\nolimits_{\rho_0\to1}^{\text{contact}}=\frac{1}{2};$$

$$6^\circ)\quad {}^{\zeta^\infty}I^{1,0}_{1,2}=\frac{2}{\pi}K_{2(1,2)}\int\limits_{\alpha=0}^{\infty}\frac{G^{1,0}_{1,2}(\alpha)}{\alpha}\frac{\mathrm{d}\alpha}{\alpha}=\frac{2}{\pi}\left(-\frac{3}{\rho_0}\right)\int\limits_{\alpha=0}^{\infty}\frac{\alpha^4}{2}\left(\frac{\rho_0^2}{\alpha^2}-\ln\left(\frac{\rho_0^2+\alpha^2}{\alpha^2}\right)\right)\frac{\rho_0}{\alpha^2}d\left(\frac{\alpha}{\rho_0}\right)$$
$$=\frac{2}{\pi}\left(\frac{-3}{\rho_0}\right)\frac{1}{\rho_0}\frac{\rho_0^4}{2}\int\limits_{\kappa=0}^{\infty}\left(1-\kappa^2\ln\left(\frac{1+\kappa^2}{\kappa^2}\right)\right)\mathrm{d}\kappa=-\rho_0^2,\ \lim\nolimits_{\rho_0\to1}^{\text{contact}}=-1;$$

$$7^\circ)\quad {}^{\zeta^\infty} I^{1,0}_{3,3} = \frac{2}{\pi} K_{3(3,3)} \int\limits_{\alpha=0}^{\infty} \frac{G^{1,0}_{3,3}(\alpha)}{\alpha} \frac{\mathrm{d}\alpha}{\alpha}$$

$$= \frac{2}{\pi} \rho_0^2 \int\limits_0^{\infty} \kappa^4 \left(\ln\left(\frac{1+\kappa^2}{\kappa^2} \right) + \frac{1}{2} \frac{1}{\kappa^4} - \frac{1}{\kappa^2} \right) \mathrm{d}\kappa = \frac{2}{5} \rho_0^2, \lim^{\text{contact}}_{\rho_0 \to 1} = \frac{2}{5};$$

$$8^\circ)\quad {}^{\zeta^\infty} I^{2,0}_{1,2} = \frac{2}{\pi} K_{2(1,2)} \int\limits_{\alpha=0}^{\infty} \frac{G^{2,0}_{1,2}(\alpha)}{\alpha} \frac{\mathrm{d}\alpha}{\alpha}$$

$$= \frac{2}{\pi} \left(\frac{-3}{2} \right) \int\limits_0^{\infty} \left(\rho_0^2 \kappa^2 + \rho_0^4 \kappa^4 \right) \left(\frac{1}{\kappa^2} + \frac{1}{1+\kappa^2} - 2 \ln\left(\frac{\kappa^2+1}{\kappa^2} \right) \right) \mathrm{d}\kappa$$

$$= -\left(\frac{\rho_0^2}{2} + \frac{3\rho_0^4}{10} \right), \lim^{\text{contact}}_{\rho_0 \to 1} = \frac{-4}{5};$$

$$9^\circ)\quad {}^{\zeta^\infty} I^{2,0}_{3,3} = \frac{2}{\pi} K_{3(3,3)} \int\limits_{\alpha=0}^{\infty} \frac{G^{2,0}_{3,3}(\alpha)}{\alpha} \frac{\mathrm{d}\alpha}{\alpha}$$

$$= \frac{2}{\pi} \int\limits_0^{\infty} \left(\rho_0^2 + \rho_0^4 \kappa^2 \right) \left(\frac{1}{2} + 3\kappa^4 \ln\left(\frac{1+\kappa^2}{\kappa^2} \right) - \frac{\kappa^4}{1+\kappa^2} - 2\kappa^2 \right) \mathrm{d}\kappa = \frac{\rho_0^2}{5} + \frac{\rho_0^4}{7}, \lim^{\text{contact}}_{\rho_0 \to 1} = \frac{12}{35}.$$

Appendix C: Numerical simulation conditions for moduli calculations to compare with estimates

For validating the presented new estimates based on considering infinite patterns in homogenization frameworks, we performed numerical simulations (in Comsol Multiphysics) by considering a 2D cell (a $x1$–$x3$ cross section of the $x2$-oriented fiber bundle) whose sides are provided of periodic boundary conditions for allowing the identification with the infinite case analytically derived in this article and for minimizing the size and the boundary effects. The representative "volume" (cross section) element (RVE), exemplified in Fig. 10, comprises a set of regularly arranged identical fibers, starting from a reference hexagonal lattice (Fig. 10b), with two different concentrations of 30% (inner circles) and 70% (outer circles) to be modified "as if" resulting from a (tensile or compressive) stretch of the RVE normally to the fiber direction. Figure 10c corresponds to a tensile stretch of $\eta = 1.2955$ (≈ 1.3) in the $x3$ direction for which the fibers get into horizontal contact when their concentration is 70% (outer circles). Figure 10a corresponds to a compressive stretch of $\eta = 1/\sqrt{3}$ along $x3$, yielding a square symmetric arrangement. The size of the RVE is taken large enough to integrate planar alignments of at least ten fibers, a minimal number to correctly estimate the global interactions when

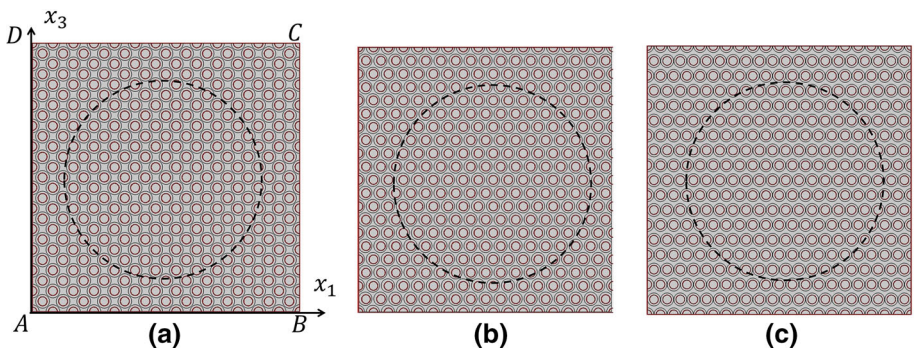

Fig. 10 The periodic cell for volume fraction of fibers equal to 30% (inner circles) and 70% (outer circles) and **a** $\eta = 1/\sqrt{3}$, **b** $\eta = 1$ and **c** $\eta = 1.3$ at contact for 70% fibers. The influence zone is marked by the dashed circle

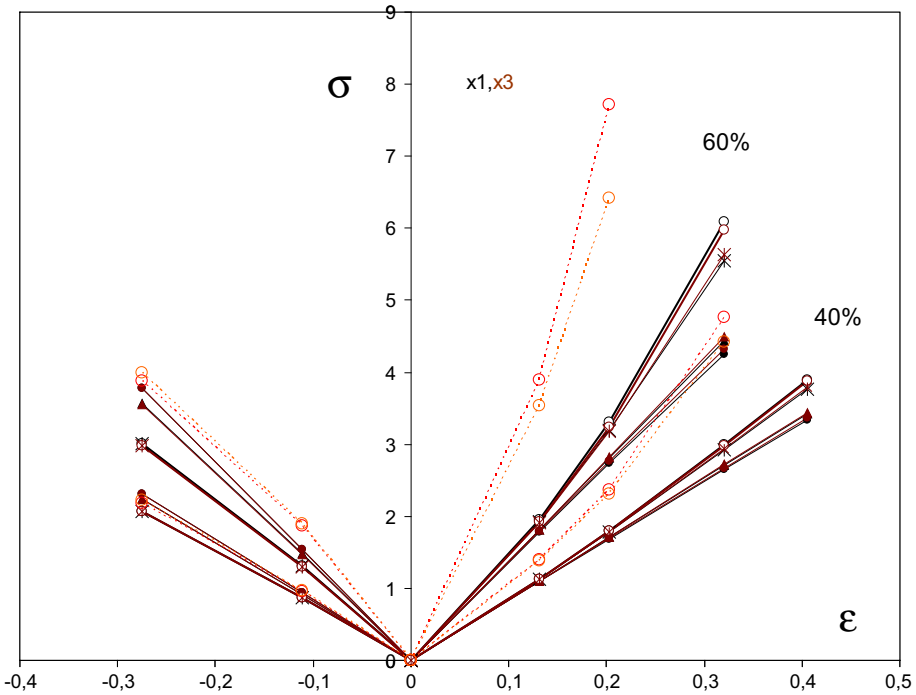

Fig. 11 A stress–strain-like representation of the obtained effective Young moduli as plotted in Fig. 8, when considering the fiber arrangement changes due to a transverse (tensile or compressive) stretch of an undeformed structure ($\eta = 1$) here taken to correspond to a regular hexagonal fiber arrangement. These plots disregard any real feature of a deformation path possibly yielding to an arrangement η from $\eta = 1$

the fiber concentration is in the non-dilute range. Each fiber arrangement corresponds to a specific value of the η, stretch-like parameter, defined from the hexagonal reference structure assigned to $\eta = 1$.
On each fiber arrangement η, two kinds of tests, a compression and a shear test, are performed in the $x1$–$x3$ cross section plane. Boundary conditions are given on the displacement vector $\boldsymbol{u}$ of R^2 whose components u and v are, respectively, in the x_1 and x_3 directions. We deduce the nomenclature of the sides of the cell from Fig. 10a: the two horizontal sides are called $\overline{AB}$ and $\overline{CD}$, $\overline{AB} = L$ and the vertical ones are $\overline{BC}$ and $\overline{DA}$, $\overline{BC} = H$. The displacements on side $\overline{AB}$ are called $\boldsymbol{u}_{AB} = (u_{AB}, v_{AB})$ and similarly for the other sides. For the determination of the Young moduli $Y1$ and $Y3$, we performed two compressions, along the two axes x_1 and x_3. Both compressions need the same boundary conditions to simulate an infinite-like structure. For allowing a compression (and not simply a translation), continuity is assigned to the horizontal (resp. vertical) displacements in the horizontal (resp. vertical) sides and anti-periodicity to the horizontal (resp. vertical) displacements in the vertical (resp. horizontal) sides. With referring to Fig. 10, we can write these conditions as $\begin{cases} u_{BC} = -u_{DA} \\ v_{BC} = v_{DA} \end{cases}$ and $\begin{cases} u_{AB} = u_{CD} \\ v_{AB} = -v_{CD} \end{cases}$. For the determination of the shear modulus $C_{1313} = C55$, we perform a shearing test along the side $\overline{BC}$. In order to obtain the same result by shearing along the two directions x_1 and x_3 for $\eta = 1/\sqrt{3}$ (square fiber arrangement) a square RVE is necessary what is not exactly fulfilled, owing to the number of fibers in the RVE. Two different boundary conditions are defined for the two possible shear tests: for shear along the x_1 direction the imposed boundary conditions are $\begin{cases} u_{BC} = u_{DA} \\ v_{BC} = v_{DA} \end{cases}$ and $\begin{cases} u_{AB} = -u_{CD} \\ v_{AB} = v_{CD} \end{cases}$; for shear along the x_3 direction, conditions become $\begin{cases} u_{BC} = u_{DA} \\ v_{BC} = -v_{DA} \end{cases}$ and $\begin{cases} u_{AB} = u_{CD} \\ v_{AB} = v_{CD} \end{cases}$. The requested moduli are calculated via a numerical measurement that is the analogous of an experimental measure, say imposing an external small displacement $\boldsymbol{u}_0$ to one of the sides and calculating the desired modulus as ratio between the computed stress and the global strain. We have considered the σ_{11} and σ_{33} components of the stress for the calculation of the Young moduli $Y1$ and $Y3$, respectively, and the $\sigma_{13} = \sigma_{31}$ component for the shear modulus $C_{1313} = C55$. This has been performed in the context of the Hooke law for linear elasticity $\sigma_{ij} = C_{ijkl}\varepsilon_{kl}$

where the strain tensor ε_{kl} is defined as $\varepsilon_{kl} = 0.5\left(u_{k,l} + u_{l,k}\right)$ with $u_{k,l} = \partial u_k/\partial x_l$, the displacement first gradient components. Obtained moduli calculations are reported in Fig. 7 for C55 and in Fig. 8 for $Y1$ and $Y3$. In the Young moduli cases, although the obtained estimates do not result from a continuously strain-due change of the fiber arrangement (various fiber arrangements are subjected to an infinitesimal strain), it is possible to mimic a stress–strain curve of which the estimated moduli are the slope. These stress–strain curves are plotted in Fig. 11 for both the numerically calculated Young moduli and the estimated ones from the four here compared estimates. The logarithmic overall strain is taken equal to $\varepsilon = \ln\sqrt{\eta}$. It is zero for the state at which η is taken (arbitrarily) to be equal to 1. Taking the hexagonal fiber arrangement as the undeformed one, two curves can be obtained whether $\eta > 1$ or $\eta < 1$ (in the latter case, the stress should have a negative sign as the strain but it is here plotted in absolute value). These data are a particular presentation of the more general ones in Fig. 8 since changing the reference state (for example starting from the square fiber arrangement as the undeformed one) can also yield other stress–strain-like curves. It is worth to precise that none of them accounts for the real features of a real deformation path (especially strain heterogeneities in the matrix) that may transform one fiber arrangement into another. These curves can nevertheless serve as indicators for first nonlinearity causes only due to changes of the fiber arrangement (everything else being invariant) in the elastic behavior of such composite materials.

References

1. Christensen, R.M., Walls, F.M.: Effective stiffness of randomly oriented fiber compositions. J. Compos. Mater. **6**, 518–531 (1972)
2. Boucher, S.: On the effective moduli of isotropic two-phase elastic composites. J. Compos. Mater. **8**, 82–89 (1974)
3. Christensen, R.M.: Mechanics of Composite Materials. Wiley, Hoboken (1979)
4. Christensen, R.M.: Isotropic properties of platelet reinforced media. J. Eng. Mater. Technol. **101**(3), 299–303 (1979)
5. Franciosi, P., El Omri, A.: Effective properties of fiber and platelet systems and related phase arrangements in n-phase heterogeneous media. Mech. Res. Commun. **38**, 38–44 (2011)
6. Franciosi, P.: Laminate system schemes for effective property estimates of architectured composites with co(dis)continuous phases. Mech. Res. Commun. **45**, 70–76 (2012)
7. Veenstra, H., Verkooijen, P.C.J., van Lent, B.J.J., van Dam, J., de Boer, A.P., Nijhof, A.H.J.: On the mechanical properties of co-continuous polymer blends: experimental and modelling. Polymer **41**(5), 1817–1826 (2000)
8. Kinney, J.H., Stölken, J.S., Smith, T.S., Ryaby, J.T., Lane, N.E.: An orientation distribution function for trabecular bone. Bone **36**(2), 193–201 (2005)
9. Clyne, T.W., Markaki, A.E., Tan, J.C.: Mechanical and magnetic properties of metal fibre networks with and without a polymeric matrix. Compos. Sci. Technol. **65**, 2492–2499 (2005)
10. Agoras, M., Lopez-Pamies, O., Ponte, Castaneda P.: Onset of macroscopic instabilities in fiber-reinforced elastomers at finite strain. J. Mech. Phys. Solids **57**, 1828–1850 (2009)
11. Broedersz, C.P., Mao, X., Lubensky, T.C., MacKintosh, F.C.: Criticality and isostaticity in fibre networks. Nat. Phys. **12**(7), 983–988 (2011)
12. Cuomo, M., Dell'Isola, F., Greco, L., Rizzi, N.L.: First versus second gradient energies for planar sheets with two families of inextensible fibres: investigation on deformation boundary layers, discontinuities and geometrical instabilities. Compos. B Eng. **115**, 423–448 (2017)
13. Placidi, L., Barchiesi, E., Turco, E., Rizzi, N.L.: A review on 2D models for the description of pantographic fabrics. Zeitschrift für angewandte Mathematik und Physik **67**(5), 121 (2016)
14. Della Corte, A., Dell'Isola, F., Esposito, R., Pulvirenti, M.: Equilibria of a clamped Euler beam (Elastica) with distributed load: large deformations. Math. Models Methods Appl. Sci. **27**(8), 1391–1421 (2017)
15. Ivan, G., Della Corte, A., Dell'Isola, F.: Dynamics of 1D nonlinear pantographic continua. Nonlinear Dyn. **88**(1), 21–31 (2017)
16. Scerrato, D., Zhurba Eremeeva, I.A., Lekszyki, T., Rizzi, N.L.: On the effect of shear stiffness on the plane deformation of linear second gradient pantographic sheet. ZAMM-Journal of Applied Mathematics and Mechanics/Zeitschrift für Angewandte Mathematik und mechanic **96**(11), 1268–1279 (2016)
17. Dell'Isola, F., Lekszycki, T., Pawlikowski, M., Grygoruk, R., Greco, L.: Designing a light fabric metamaterial being highly macroscopically tough under directional extension: first experimental evidence. Zeitschrift für angewandte Mathematik und Physik **66**(6), 3473–3498 (2015)
18. Dell'Isola, F., Cuomo, M., Greco, L., Della Corte, A.: Bias extension test for pantographic sheets: numerical simulations based on second gradient shear energies. J. Eng. Math. **103**(1), 127–157 (2017)
19. Dell'Isola, F., Giorgio, I., Andreaus, U.: Elastic pantographic 2D lattices: a numerical analysis on static response and wave propagation. Proc. Est. Acad. Sci. **64**(3), 219–225 (2015)
20. Dell'Isola, F., Giorgio, I., Pawlikowski, M., Rizzi, N.L.: Large deformations of planar extensible beams and pantographic lattices: heuristic homogenization, experimental and numerical examples of equilibrium. Proc. R. Soc. A **472**(2185), 20150790 (2016)
21. Rahali, Y., Giorgio, I., Ganghoffer, J.F., Dell'Isola, F.: Homogenization à la Piola produces second gradient continuum models for linear pantographic lattices. Int. J. Eng. Sci. **97**, 148–172 (2015)
22. Andreaus, U., Sawczuk, A.: Deflection of elastic-plastic frames at finite spread of yielding zones. Comput. Methods Appl. Mech. Eng. **39**(1), 21–35 (1983)

23. Andreaus, U., D'Asdia, P.: Displacement analysis in elastic-plastic frames at plastic collapse. Comput. Methods Appl. Mech. Eng. **42**(1), 19–35 (1984)
24. Andreaus, U., D'Asdia, P.: Incremental analysis of elastic-plastic frames at finite spread of yielding zones. Eng. Fract. Mech. **21**(4), 827–839 (1985)
25. Andreaus, U., D'Asdia, P.: An incremental procedure for deformation analysis of elastic-plastic frames. Int. J. Numer. Methods Eng. **26**(4), 769–784 (1988)
26. König, J.A.: An iterative method of evaluation of elastic-plastic deflections of hyperstatic framed structures. Ingenieer-Archiv **55**(3), 202–212 (1985)
27. Rangelov, T.V., Manolis, G.D., Dineva, P.S.: Elastodynamic fundamental solutions for certain families of 2d inhomogeneous anisotropic domains: basic derivations. Eur. J. Mech. A/Solids **24**, 820–836 (2005)
28. Manolis, G.D., Makra, K., Dineva, P.S., Rangelov, T.V.: Seismic motions in a non-homogeneous soil deposit with tunnels by a hybrid computational technique. Earthq. Struct. **5**(2), 161–205 (2013)
29. Chen, Z., Jeffrey, R.G., Pandurangan, V.: The far-field deformation caused by a hydraulic fracture in an inhomogeneous elastic half-space. Int. J. Solids Struct. **130**, 220–231 (2018)
30. Willis, J.R., Acton, J.R.: Overall elastic moduli of a dilute suspension of spheres. Q. J. Mech. Appl. Mech. **29**, 163–177 (1976)
31. Kröner, E.: Modified Green functions in the theory of heterogeneous and/or anisotropic linearly elastic media. In: Weng, G.J., Taya, M., Abe, H. (eds.) Micromechanics and Inhomogeneity, pp. 197–211. Springer, New York (1990)
32. Lebensohn, R.A., Tome, C.N.: Anisotropic approach for the simulation of plastic deformation and texture development of polycrystals. Acta Metall. **41**, 2611–2624 (1993)
33. El Omri, A., Fennan, A., Sidoroff, F., Hihi, A.: Elastic-plastic homogenization for layered composites. Eur. J. Mech. A/Solids **19**, 585–601 (2000)
34. Ponte Castaneda, P., Willis, J.R.: The effect of spatial distribution on the effective behaviour of composite materials and cracked media. J. Mech. Phys. Solids **43**(12), 1919–1951 (1995)
35. Bornert, M., Stolz, C., Zaoui, A.: Morphologically representative pattern-based bounding in elasticity. J. Mech. Phys. Solids **44**(3), 307–331 (1996)
36. Franciosi, P.: The boundary-due terms in the Green operator of inclusion patterns from distant to contact and to connected situations using Radon transforms: illustration for spheroid alignments in isotropic media. Int. J. Solids Struct. **47**(2), 304–319 (2010)
37. Franciosi, P., Barboura, S., Charles, Y.: Analytical mean Green operators/Eshelby tensors for patterns of coaxial finite long or flat cylinders in isotropic matrices. Int. J. Solids Struct. **66**(1), 1–19 (2015)
38. Eshelby, J.D.: The determination of the elastic field of an ellipsoidal inclusion and related problems. Proc. R. Soc. Lond. A **421**, 379–396 (1957)
39. Berveiller, M., Fassi-Ferhi, O., Hihi, A.: The problem of two plastic and heterogeneous inclusions in an anisotropic medium. Int. J. Eng. Sci. **25**(6), 691–709 (1987)
40. Kouris, D., Tsuchida, E.: On the elastic interaction between two fibres in a continuous fibre composite under thermal loading. Mech. Mater. **12**, 131–146 (1991)
41. Anttreter, T., Fisher, F.D.: The stress state around two spatially arranged ellipsoidal inclusions. A case study for high-speed tool steel. Comput. Mater. Sci. **7**, 247–252 (1996)
42. Franciosi, P., Lormand, G.: Using the Radon transform to solve inclusion problems in elasticity. Int. J. Solids Struct. **41**(3/4), 585–606 (2004)
43. Gel'fand, I.M., Graev, M.I., Vilenkin, NYa.: Generalized Functions, Integral Geometry and Representation Theory, vol. 5. Academic Press, New York (1966)
44. Natterer, F.: The Mathematics of Computerized Tomography. Wiley, Stuttgart (1986)
45. Ramm, A.G., Katsevitch, A.I.: Radon Transform and Local Tomography. CRC Press, Boca Raton (1996). ISBN 0849394929
46. Helgason, S.: The Radon Transform, Progress in Mathematics, vol. 5. Birkhausser, Boston (1980)
47. Willis, J.R.: Interfacial stresses induced by arbitrary loading of dissimilar elastic half-spaces joined over a circular region. IMA J. Appl. Math. **7**, 179–197 (1971)
48. Wang, C.-Y.: Elastic fields produced by a point source in solids of general anisotropy. J. Eng. Math. **32**, 41–52 (1997)
49. Pan, E., Tonon, F.: Three dimensional Green's functions in anisotropic piezoelectric solids. Int. J. Solids Struct. **37**, 943–958 (2000)
50. Meisner, M.J., Kouris, D.A.: Interaction of two elliptic inclusions. Int. J. Solids Struct. **32**, 451–466 (1995)
51. Ju, J.W., Sun, L.Z.: A novel formulation for the exterior point Eshelby's tensor of an ellipsoidal inclusion. J. Appl. Mech. **66**, 570–574 (1999)
52. Nakasone, Y., Nishiyama, H., Nojiri, Y.: Numerical equivalent inclusion method: a new computational method for analyzing stress fields in and around inclusions of various shapes. Mater. Sci. Eng. A **285**, 229–238 (2000)
53. Kushch, V.I., Shmegera, S.V., Buryachenko, V.A.: Interacting elliptic inclusions by the method of complex potentials. Int. J. Solids Struct. **42**, 5491–5512 (2005)
54. Zheng, Q.S., Zhao, Z.H., Du, D.X.: Irreducible structure, symmetry and average of Eshelby's tensor field in isotropic elasticity. J. Mech. Phys. Solids **54**(2), 368–383 (2006)
55. Franciosi, P.: Mean and axial Green and Eshelby tensors for an inclusion with finite cylindrical shape. Mech. Res. Commun. **59**, 26–36 (2014)
56. Franciosi, P.: On the modified Green operator integral for polygonal, polyhedral and other non-ellipsoidal inclusions. Int. J. Solids Struct. **42**(11/12), 3509–3531 (2005)
57. Franciosi, P.: A Decomposition method for obtaining global mean Green operators of inclusions patterns. Application to parallel infinite beams in at least transversally isotropic media. Int. J. Solids Struct. (2018). https://doi.org/10.1016/j.ijsolstr.2018.04.005
58. Hasegawa, H., Lee, G., Mura, T.: The stress field caused by a circular-cylindrical inclusion. J. Appl. Mech. **59**, 107–114 (1992)

59. Wu, L., Du, S.Y.: The elastic field caused by a circular cylindrical inclusion—part II: inside the region $x1^2 + x2^2 > a^2$. J. Appl. Mech. **62**, 585–589 (1995)
60. Mura, T.: Micro-mechanics of Defects in Solids, 2nd edn. Martinus Nijhoff, Dordrecht (1987)
61. Cherkaev, A.: Variational Methods for Structural Optimization, Applied Mathematical Sciences. Springer, Berlin (2000)
62. Buryachenko, V.A.: Multiparticle effective field and related methods in micromechanics of composite materials. Appl. Mech. Rev. **54**, 1–47 (2001)
63. Buryachenko, V.A.: Micromechanics of Heterogeneous Materials. Springer, Berlin (2007)
64. Buryachenko, V.A., Kushch, V.I., Roy, A.: Effective thermoelastic properties of ramdom structure composites reinforced by the clusters of deterministic structures (application to clay composites). Acta Mech. **192**(1–4), 135–167 (2007)
65. Franciosi, P., Charles, Y.: Mean Green operator and Eshelby tensor for hemispherical inclusions and bi-material spherical inclusions in infinite spaces. Mech. Res. Commun. **75**, 57–66 (2016)
66. Franciosi, P.: Transversally isotropic Magneto-electro-elastic composites with co-(dis)continuous phases. Int. J. Solids Struct. **50**, 1013–1031 (2013)
67. Walpole, L.J.: Elastic behavior of composites materials. Adv. Appl. Mech. **21**, 169–242 (1981)
68. Franciosi, P., Lebail, H.: Anisotropy features of phase and particle spatial pair distributions in various matrix/inclusions structures. Acta Mater. **52**, 3161–3172 (2004)
69. Eremeyev, V.A., Dell'Isola, F., Boutin, C., Steigmann, D.: Linear pantographic sheets: existence and uniqueness of weak solutions. J. Elast. **1**, 1–22 (2017)
70. Altenbach, H., Eremeyev, V.A.: On the elastic plates and shells with residual surface stresses. Proc. IUTAM **21**, 25–32 (2017)
71. Andreaus, U., Chiaia, B., Placidi, L.: Soft-impact dynamics of deformable bodies. Contin. Mech. Thermodyn. **25**(2–4), 375,398 (2013)
72. Spagnuolo, M., Barcz, K., Pfaff, A., dell'Isola, F., Franciosi, P.: Qualitative pivot damage analysis in aluminum printed pantographic sheet: numerics and experiments. Mech. Res. Commun. **83**, 47–52 (2017)